

1 **Title:** Pattern separation of spiketrains by individual granule cells of the dentate gyrus

2 **Short Title:** Temporal pattern separation in the dentate gyrus

3 **Authors:** Antoine D. Madar\*<sup>1</sup>, Laura A. Ewell\*<sup>2</sup>, Mathew V. Jones<sup>1</sup>

4 \* These authors contributed equally to the manuscript.

## 5 **Authors affiliations**

6 <sup>1</sup>Department of Neuroscience, University of Wisconsin-Madison, Madison, WI 53705, USA

7 <sup>2</sup>Laboratory for Experimental Epileptology and Cognition Research, Department of  
8 Epileptology, University of Bonn, Bonn, Germany

## 9 **Corresponding authors**

10 Mathew V. Jones ([mathewjones@wisc.edu](mailto:mathewjones@wisc.edu))

11 Antoine D. Madar ([madar@wisc.edu](mailto:madar@wisc.edu))

## 12 **Author contributions**

13 Conceptualization: MVJ, LAE. Data curation: LAE, ADM. Formal analysis: MVJ, ADM.

14 Funding acquisition: MVJ, LAE, ADM. Investigation/data collection: LAE, ADM.

15 Methodology: MVJ, LAE, ADM. Project administration: MVJ, LAE, ADM. Resources: N/A.

16 Software: MVJ, ADM. Supervision: MVJ. Validation: MVJ, LAE, ADM. Visualization: MVJ,

17 LAE, ADM. Writing – original draft: ADM. Writing – review & editing: MVJ, LAE, ADM.

18

## 19 **Funding**

20 This work was supported by the University of Wisconsin Institute for Clinical and Translational

21 Research (M.V.J.; NIH/NCATS UL1TR000427) and Lily's Fund for Epilepsy Research

22 (A.D.M.; 2015 fellow).

## 23 **Abbreviations**

24 GC, granule cell; FS, fast-spiking interneuron; PP, perforant-path; R, Pearson's correlation  
25 coefficient; NDP, normalized dot product; SF, scaling factor; SR, spiking reliability;  $R_w$ ,  
26 spiketrain reliability

27

## 28 **Abstract**

29

30 Pattern separation is a process that minimizes overlap between patterns of neuronal activity  
31 representing similar experiences. Theoretical work suggests that the dentate gyrus (DG) performs  
32 this role for memory processing but a direct demonstration is lacking. One limitation is the  
33 difficulty to measure DG inputs and outputs simultaneously. To rigorously assess pattern  
34 separation by DG circuitry, we used mouse brain slices to stimulate DG afferents and  
35 simultaneously record granule cells (GCs). Output spiketrains of GCs are more dissimilar than  
36 their input spiketrains, demonstrating for the first time temporal pattern separation at the level of  
37 single neurons in DG. This phenomenon occurs on millisecond to second timescales through  
38 different neural codes and is not explained by simple noise. Pattern separation is cell-type  
39 specific and larger in GCs than in fast-spiking interneurons. Finally, different GCs process  
40 spiketrains differently, a mechanism that likely helps to separate patterns at the population level.

41

## 42 **Introduction**

43

44 How does the brain allow us to discriminate between similar events in our past? This question is  
45 a central challenge in the neurobiology of memory and remains elusive. To prevent confusion

46 between memories that share similar features, the brain needs to store distinct activity patterns to  
47 represent distinct memories. In the influential Hebb-Marr framework of episodic memory (1, 2),  
48 representations are stored in area CA3 of hippocampus, an auto-associative network where  
49 plastic recurrent excitatory connections facilitate recall of stored patterns in response to partial  
50 cues (1, 3). However, strong recurrent excitation severely limits the number of patterns that can  
51 be stored without overlap (3, 4). Such overlap would lead, when a partial cue common to several  
52 patterns is presented, to the reactivation of many patterns and thus to confusion or confabulation.  
53 To avoid these interferences, the Hebb-Marr framework proposes that redundancy between input  
54 patterns is reduced before they are stored. This process of transforming similar input patterns  
55 into less similar output patterns is termed "pattern separation" (4, 5).

56 Theoretical models suggest that the dentate gyrus (DG) performs pattern separation of  
57 cortical inputs before sending its differentiated outputs to CA3 (2, 3). Indeed, DG is ideally  
58 located to do this, receiving signals via the major projection from entorhinal cortex (EC), the  
59 perforant path (PP), and sending signals to CA3 via granule cells (GCs) axons (6). In addition,  
60 behavioral studies have shown that DG lesions impair mnemonic discrimination (7-10).  
61 However, although experimental reports have concluded that pattern separation is performed by  
62 DG (11-15), they only directly show that similar environments or events are represented  
63 differently in the DG. The separation could be done by upstream structures and simply be  
64 reported by DG. Hence, it is still unknown whether DG itself performs pattern separation. A  
65 rigorous demonstration would require simultaneous knowledge of the inputs arriving at DG and  
66 the processed outputs from DG to CA3 (5).

67 Another difficulty in studying pattern separation is in defining the nature of "activity  
68 patterns". Previous studies have focused on spatial patterns of "active neurons", with little

69 reference to the dynamics of neural activity. For example, computational models predict that DG  
70 separates overlapping populations of active EC neurons into less overlapping populations of  
71 active GCs (4, 16-19). Immediate-early genes (IEG) expression studies have confirmed that  
72 distinct events drive plasticity in different populations of GCs (13, 14, 20) and that overlap in  
73 these representations causes mnemonic interference (21). In contrast, *in vivo* single-unit  
74 recordings in the DG found that similar contexts are represented by the same population of active  
75 neurons, but differences are encoded by different spatially tuned firing patterns (11, 12).

76         These conflicting results show that pattern separation can correspond to different  
77 computations depending on the type of patterns investigated, and that multiple forms of pattern  
78 separation could in theory be implemented by DG (5). For example, because *in vivo* recordings  
79 suggest that the same neurons are used to code different environments (11, 12), it is possible that  
80 pattern separation is performed at the level of single GCs, each disambiguating the activity  
81 patterns that it receives. Such disambiguation could be done by changing firing rates, or  
82 alternatively, by changing spike timing. Previous experimental investigations of pattern  
83 separation in DG examined population vectors of place fields averaged over minutes (11, 12),  
84 but place cells also carry information at shorter timescales (22-24). So far, pattern separation has  
85 not been well characterized on the scale of milliseconds, and never where patterns are explicitly  
86 afferent and efferent trains of action potentials.

87         Here, we test the hypothesis that DG performs pattern separation of cortical spiketrains,  
88 through single GCs, on the millisecond to second timescale. We designed a novel pattern  
89 separation assay in acute brain slices to take advantage of the experimental control afforded to  
90 slice electrophysiology. Input spiketrains of varying similarities were fed into DG via its  
91 afferents, and the output of a GC was simultaneously recorded, allowing the first direct measure

92 of pattern separation (by comparing input similarity versus output similarity), on timescales  
93 relevant to neuronal encoding and synaptic plasticity (23, 25-27).

94

## 95 **Results**

96

### 97 **Temporal pattern separation by individual dentate granule cells**

98 A direct test of pattern separation in single GCs requires knowledge of the similarity between  
99 input patterns arriving via the PP, and comparison with the similarity between GC output  
100 patterns. Here, we define input and output patterns as rasters of spiketrains. Unless otherwise  
101 specified, the similarity between two spiketrains was assessed by computing their pairwise  
102 Pearson's correlation coefficient ( $R$ ) using a binning window  $\tau_w$  of 10 ms. We generated sets of  
103 Poisson input spiketrains (simulating trains of incoming cortical action potentials), with each set  
104 having an average correlation  $R_{\text{input}}$  (**Fig 1A** and **Materials and methods – Pattern separation**  
105 **experiments**). We then recorded the spiking responses of GCs to these sets of input trains  
106 delivered to PP fibers (**Fig 1B-C**) (102 recording sets from 28 GCs), allowing us to compute the  
107 average output correlation ( $R_{\text{output}}$ ) (**Fig 2A-B**).

108 For every recording set,  $R_{\text{output}}$  was lower than the  $R_{\text{input}}$  of the associated input set,  
109 indicating a decorrelation of the output spiketrains compared to their inputs (**Fig 2C**). These  
110 results are the first direct experimental evidence that single GCs, the output neurons of DG,  
111 exhibit pattern separation. The effective decorrelation, defined as the difference between  $R_{\text{input}}$   
112 and  $R_{\text{output}}$ , was statistically significant for every input set, but was larger when input spiketrains  
113 were highly correlated (**Fig 2D**). This is consistent with the role of DG in discriminating between  
114 similar memories more than already dissimilar ones (8). Note, however, that the decorrelation

115 normalized to  $R_{\text{input}}$  is invariant: whatever the input set, the output trains were always  
116 decorrelated to about 70% of  $R_{\text{input}}$  (**Fig 2E**). Such invariance suggests that the same  
117 decorrelating mechanism is used on all input sets.

118 Pearson's correlation coefficient is often used to quantify the similarity between neural  
119 activity patterns in computational models (17) and in experimental recordings (11, 12). However,  
120 the original Hebb-Marr framework theorized pattern separation as the orthogonalization of the  
121 input patterns (1, 5, 28). As a result, the terms "decorrelation" and "orthogonalization" are often  
122 conflated in the literature, even though they are not mathematically equivalent and have a non-  
123 linear relationship (**S1 Fig** and see **Materials and methods – Similarity metrics**). For instance,  
124 pairs of spiketrains can be uncorrelated ( $R = 0$ ) without being orthogonal, or can be orthogonal  
125 without being uncorrelated (**Fig 3A-C** and **S1 Fig**). To determine whether output spiketrains of  
126 GCs are truly orthogonalized, we considered spiketrains as vectors and computed the normalized  
127 dot product (NDP) between pairs of spiketrains to assess their similarity (**Fig 3A, C**). For every  
128 recording set,  $\text{NDP}_{\text{output}}$  was lower than  $\text{NDP}_{\text{input}}$ , indicating that the angle between output  
129 spiketrains was closer to a right angle (i.e., orthogonal) than their inputs (**Fig 3D-E**).

130 Vectors can differ by their angle, but also by their norm, which in the case of spiketrains  
131 is purely dependent on the binwise firing rates. In other words, even if neurons fire in the same  
132 time bins (relative to the start of each sweep), the number of spikes per bin can be different, as  
133 quantified by the ratio between their norms (scaling factor, SF) (**Fig 3A, C** and **S1 Fig**). Our  
134 results show that for very similar inputs,  $\text{SF}_{\text{output}}$  is slightly lower than  $\text{SF}_{\text{input}}$  for most recording  
135 sets (**Fig 3F**). This indicates that variations in the binwise firing rate of single GCs in response to  
136 similar inputs is a potential, but weak, mechanism of pattern separation at the 10 ms timescale.

137 As a whole, these results are the first demonstration that input spiketrains are decorrelated  
138 in the DG at the level of single GCs, and that this form of pattern separation is mediated by high  
139 levels of orthogonalization and weak levels of scaling. As a result, even though R, NDP and SF  
140 are not linearly related in theory, R and NDP have a near linear relationship in our dataset, as  
141 opposed to R and SF (**S1 Fig E-F**).

142

### 143 **Relevant timescales of temporal pattern separation**

144 To measure the similarity of spiketrains we have used metrics that require binning them in time  
145 windows of a prespecified size ( $\tau_w$ ). Because the timescales meaningful for the brain remain  
146 uncertain, it is important to assess the separation of spiketrains for different  $\tau_w$ . Our analysis  
147 shows that pattern separation, measured through R or NDP, is more pronounced at short  
148 timescales (e.g. 5 ms) than at longer ones ( $\geq 100$  ms) (**Fig 4A-B**). However, although scaling is  
149 weak at short timescales it allows DG to perform pattern separation at longer ones (0.5-2 s)  
150 through variation of the firing rate (**Fig 4C**).

151 Because many previous studies suggest that spiketrains can carry information directly  
152 through the timing of individual spikes (25-27), we also assessed the similarity between  
153 spiketrains using SPIKE, a binless metric purely based on spike times (29). Our results show that  
154 input spiketrains with very similar spike times relative to their sweep start (defined here as  
155 spiketrains with a high degree of *synchrony*, see **Materials and methods – Similarity metrics**),  
156 are transformed into significantly less synchronous outputs, thereby confirming that temporal  
157 pattern separation occurs through spike timing modifications in single GCs (**Fig 4D**).

158

### 159 **Mechanism of temporal pattern separation**

160 To determine what mechanisms might support temporal pattern separation in GCs, it is necessary  
161 to understand its dynamics first. Limiting our analysis to the first presentation of an input set  
162 revealed that outputs were already significantly decorrelated (**Figure 5A-B**). This shows that the  
163 separation mechanism is fast, consistent with the fact that the brain generally does not have the  
164 opportunity to average repeated signals. In addition, analysis of the last presentation revealed  
165 only modestly more separation than for the first one, and only for high input correlations (**Figure**  
166 **5C**), suggesting that learning to recognize the input pattern is not critical.

167 Because the mechanism for temporal pattern separation is fast and does not require  
168 learning, we asked first whether intrinsic properties of GCs could play a role. Linear regression  
169 analysis revealed that the membrane capacitance, resistance, time constant as well as the resting  
170 membrane potential are not predictors of decorrelation in GCs (see low  $R^2$  in **Table 1**). Another  
171 hypothesis is that randomness in neuronal responses drives the decorrelation. Indeed, when the  
172 same input spiketrain is repeated (e.g.  $R_{\text{input}} = 1$ ) the output spiket trains are not well correlated  
173 (as shown by the mean spiketrain reliability  $R_w$ ) (**Figure 6A**), consistent with well-known trial-  
174 to-trial variability in single neuron responses (25, 30, 31). Theoretical investigation of pattern  
175 separation often relies on some sort of random process such as probabilistic neuronal activation  
176 (4) or stochastic firing (32), which suggests that “neural noise” is a likely contributor to any form  
177 of pattern separation. However, because “neural noise” can cover multiple different definitions  
178 and phenomena (30), determining its role in a complex computation is not trivial.

179 Although the noisiness in neural communication is often understood as the unreliability  
180 of spiking after a single input spike, and the jitter of the delay between an input spike and an  
181 output spike (33), to our knowledge it had never been characterized in GCs before. Hence, we  
182 assessed this spike-wise noise in our recordings (**Fig 6B**, **S2 Fig**, and **Materials and methods** –



183 **Noise parameters**) and asked whether it can predict the degree of decorrelation by GCs. First,  
184 linear regression analysis shows no clear relationship, the spiking reliability (SR) being a  
185 mediocre predictor at best (**S3 Fig, Table 2**). Moreover, the average firing rate of a GC output  
186 set (a measure directly dependent on SR) is not well correlated with the degree of decorrelation  
187 either (**Table 3, S5B Fig**). Thus, even though a relationship might be expected between firing  
188 rates and pairwise spiketrains similarity due to higher rates leading to increased probability of  
189 spiking close in time (but see **Materials and methods – Similarity metrics**), temporal pattern  
190 separation in GCs is not achieved merely because their output spiketrains are sparser than their  
191 inputs.

192 To more carefully test the hypothesis that random spiking failures and delays support  
193 fast temporal pattern separation, we produced a shuffled data set and a simulated data set only  
194 governed by spike-wise noise statistics comparable to the original data (**S2 Fig and Materials**  
195 **and methods – Simulated and shuffled data**).  $R_{\text{output}}$  was significantly higher in the original  
196 data (**Fig 6** and **S4 Fig**), showing that purely random processes yield greater levels of separation  
197 than real GCs, especially for highly similar inputs (**Fig 6E** and **S4B Fig**).

198 In addition to the spike-wise noise, we considered neural noise at the level of spiketrains  
199 using  $R_w$  (**Fig 6A**). It characterizes the more complex notion of "spiketrain reliability", that is the  
200 ability of a neuron to reproduce the same output spiketrain in response to repetitions of the same  
201 input spiketrain. It is not dependent on intrinsic cellular properties (**Table 1**) and only modestly  
202 determined by the spike-wise noise (**Table 2**), suggesting that the rather low  $R_w$  of GCs is the  
203 expression of more complex noisy biophysical processes. Consistently,  $R_w$  was significantly  
204 lower for shuffled and simulated data than in real GCs (**Fig 6D-E** and **S4C Fig**). This indicates

205 that the output spiketrains of GCs are more reliable than if their output was entirely determined  
206 by simple random processes.

207 Overall, the lower  $R_{\text{output}}$  and  $R_w$  distributions of random datasets compared to GCs (**Fig**  
208 **6**) clearly show that simple noise cannot fully underlie the operations performed by GCs on input  
209 spiketrains. It also suggests that there might be an unavoidable trade-off between achieving  
210 pattern separation and reliable information transmission about input spiketrains. To further test  
211 this, we looked at the relationship between  $R_w$  and decorrelation levels in individual GC  
212 recordings and found a strong anticorrelation (**Fig 7A** and **Table 3**). This is clear evidence that a  
213 biological process leading to sweep-to-sweep variability is a powerful mechanism for temporal  
214 pattern separation in DG. However, it is not the only source of decorrelation. Indeed, when  
215 averaging out the variability between spiketrains associated to the same input, a significant level  
216 of decorrelation is still detected (**Fig 7B-E**). In addition, high levels of pattern separation are  
217 achieved in a single sweep (**Fig 5**). This indicates that even if the output spiketrains were  
218 perfectly the same from sweep to sweep, they would still be decorrelated compared to their  
219 inputs. This makes our discovery that sweep-to-sweep variability is strongly related to temporal  
220 pattern separation (**Fig 7A**) even more surprising.

221 Taken together, these results suggest that complex biophysical mechanisms allow GCs to  
222 balance temporal pattern separation and reliable signaling about their inputs.

223

### 224 **Fast-spiking interneurons exhibit less temporal pattern separation than GCs**

225 Any brain system might perform either pattern separation or pattern convergence to some degree  
226 (5). Thus, GCs are unlikely to be the only neurons to exhibit temporal pattern separation of  
227 spiketrains. However, we would expect pattern separation to be at its greatest in GCs, at least

228 among DG cells, because they are the output neurons of the DG. To test this hypothesis, we  
229 performed the same pattern separation assay while recording from fast-spiking interneurons (FS)  
230 of the DG instead or in addition to a GC (20 recording sets were collected on 4 FS) (**Fig 8**). We  
231 chose FS interneurons because, like GCs, they receive strong input from the PP (34). The  
232 distributions of  $R_{\text{output}}$  were significantly different between the two cell types, with the  $R_{\text{output}}$  of  
233 simultaneously recorded GCs always lower than their corresponding FS (**Fig 8D**). This indicates  
234 that FS perform lower levels of decorrelation than GCs.

235 On the other hand,  $R_w$  is significantly higher in FS (**Fig 8E**), illustrating again the trade-  
236 off between spiketrain reliability and separation. Surprisingly, in FS, the relationship between  $R_w$   
237 and decorrelation follows exactly the same regression line as in GCs (**Fig 7A, Table 3**),  
238 suggesting that this trade-off is universal across cell-types.

239 FS displayed bursting (i.e. more than one output spike between two input spikes) never  
240 seen in GCs (34) (**Fig 8C and S5A, S5C Fig**) and thus had higher firing rates than GCs (**S5B, D**  
241 **Fig**). Higher firing rates in FS lead to higher correlations between their output spiketrains (**S5B**  
242 **Fig**). We tested whether the bursting was the reason that FS perform less pattern separation than  
243 GCs by removing all spikes in a burst except the first one from the FS data set (**S5C Fig**). The  
244 resulting dataset ("non-burst" FS: nbFS) had a much lower mean firing rate than FS (**S5D Fig**).  
245 However, the degree of correlation of output spiketrains in nbFS was still significantly higher  
246 than in GCs (**S5E Fig**). Therefore, bursting and high firing rates are not sufficient to explain the  
247 difference between FS and GCs in their ability to separate spiketrains. Interestingly,  $R_w$  was also  
248 still higher in nbFS than in GCs (**S5F Fig**), showing that the greater ability of FS to reliably  
249 transmit information is not a mere consequence of bursting or high firing rates.

250           Although FS show less pattern separation than GCs, it is interesting that they do exhibit  
251 some amount of separation, as opposed to pattern convergence (5) which one could have  
252 expected from their reputation of having a much more reliable and precise spiking behavior than  
253 principal neurons (33, 35). The high fidelity in relaying input spikes (33) might still explain the  
254 difference in pattern separation ability between FS and GCs, although, to our knowledge, they  
255 had never been formally compared. We thus first confirmed the idea that FS show much less  
256 spike-wise noise than GCs (**S6 Fig**). Then, linear regressions revealed that SR is a good predictor  
257 of FS decorrelation performance and  $R_w$  (**Table 2**). Surprisingly, the membrane resistance was  
258 also a good predictor (**Table 1**). Thus, contrarily to GCs, FS pattern separation behavior is  
259 strongly and linearly determined by some intrinsic and spike-wise properties, even though it is in  
260 principle hazardous to anticipate complex neuronal operations from such low-level  
261 characteristics, as our previous analysis on GCs illustrated.

262           Overall, these results show that FS perform temporal pattern separation, but to a lower  
263 degree than GCs, likely because of their intrinsic properties that allow them to relay information  
264 very reliably.

265

### 266 **GCs perform temporal pattern separation through distinct operations on input patterns**

267 Pattern separation is typically considered as a population-coding process (5), suggesting that  
268 different GCs should take on distinct roles in coding different patterns. To compare GCs to each  
269 other, we first assessed the correlation between spiketrains from different cells (not recorded  
270 simultaneously) in response to the same input set (**Fig 9A1**). The average correlation  $R_{\text{cell-to-cell}}$  is  
271 not dependent on  $R_{\text{input}}$  and is broadly distributed but skewed towards 0 (**Fig 9A2**). This suggests  
272 that different GCs have a general tendency not to fire the same way in response to the same input

273 spiketrain. On the contrary, FS responses are more consistent between neurons, and FS activity is  
274 also poorly correlated with simultaneously recorded GCs (**Fig 9A3**).

275       Next, we analyzed whether GCs perform pattern separation to the same degree on all  
276 pairs of input spiketrains, and compared the amount of decorrelation between different GCs (**Fig**  
277 **9B**). Individual GCs did not process all input spiketrains in the same way, as demonstrated by the  
278 small but significant variability in effective decorrelation for different pairs of input spiketrains  
279 (**Fig 9B2**). This variability profile was then used as a fingerprint to be compared across cells that  
280 processed the same input set. Our results suggest that different GCs, even from the same animal,  
281 can perform pattern separation of the same input spiketrains quite differently. Furthermore, the  
282 way pattern separation is performed from GC to GC is more variable and more likely to be  
283 different for highly similar input (**Fig 9B3**), which is when pattern separation is theoretically  
284 most needed.

285       These results show that there is variability between different GCs in the way they process  
286 and decorrelate input spiketrains, which cannot be attributed to variability in intrinsic cellular  
287 properties (**Table 1**).

288

## 289 **Discussion**

290

291 We report that similar input spiketrains are transformed, in GCs, into less similar output  
292 spiketrains. Our findings provide the first experimental demonstration that a form of pattern  
293 separation is performed within the DG itself and exhibited at the level of single neurons at  
294 different timescales through different neural codes. Not all DG neurons perform this computation  
295 to the same high degree as GCs, the output neurons of DG to CA3. Finally, temporal pattern

296 separation does not purely result from simple neural noise, but is subject to variability within and  
297 between neurons that likely supports pattern separation at the population level.

298

### 299 **A novel way to test pattern separation**

300 In contrast to *in vivo* experiments that have difficulty identifying recorded units with certainty  
301 (36-39) and simultaneously recording the direct inputs of these units (11-15), *in vitro* brain slices  
302 that preserve the lamellar connections of the hippocampus offer a more accessible platform. For  
303 example, a similar experimental setup to ours was used to show that spatially segregated inputs  
304 are represented by distinct spatiotemporal patterns in populations of DG neurons (40, 41).  
305 However, our study is the first to perform an experimental analysis of pattern separation within  
306 DG by manipulating the similarity of the inputs and comparing it to the similarity of the outputs.  
307 Such a systematic approach had so far only been done in computational studies (42). Although a  
308 rigorous comparison is impossible because the activity patterns considered were defined  
309 differently, the general pattern separation behavior of those models is consistent with our results  
310 (**Fig 2C-D**).

311 Studies investigating pattern separation also often differ in the way they measure the  
312 similarity between activity patterns. Many methods have been designed to assess similarity  
313 between pairs of spiketrains (43-45), each assuming a different definition of similarity. Because  
314 we don't know which definition is used by the brain, and given the possibility that multiple ones  
315 are relevant, it is important to maintain an agnostic approach. Our study is the first to  
316 systematically test pattern separation by considering several similarity measures that span a wide  
317 range of potential neural codes (see **Materials and methods – Similarity metrics**). The fact that  
318 conceptually different metrics lead to converging results bolsters our conclusion that pattern

319 separation occurs within DG at the level of single GCs. Experiments linking mnemonic  
320 discrimination by animals with various potential forms of neural pattern separation will help  
321 pinpoint which computations are actually used in episodic memory.

322

### 323 **Pattern separation through "time" codes.**

324 Until now, most studies of pattern separation in the DG assumed that neural activity patterns  
325 were ensembles of ON/OFF neurons (3, 4, 13, 14, 16), sometimes considering a rate code  
326 averaged over minutes in addition to this population code (11, 12, 19, 32). Because neurons carry  
327 information at timescales shorter than minutes (22-26), and because the sparse firing of active  
328 GCs during a brief event (15, 46, 47) precludes an efficient rate code (25), we studied pattern  
329 separation at sub-second timescales.

330         Relevant scales are given by the time constant over which neurons can integrate synaptic  
331 inputs (23): 10-50 ms for GCs and ~100ms for the "reader" CA3 pyramidal cells. Windows of  
332 ~10 ms and ~100 ms, corresponding to gamma and theta rhythms respectively, have been shown  
333 to organize CA neuronal assemblies (22, 23, 48, 49). In the DG, spiketrains recorded in similar  
334 environments were less synchronous than in CA3 when considering 30-300 ms windows (11). In  
335 addition, due to specific network properties allowing persistent activity, the DG might also  
336 integrate information over longer time epochs on the order of seconds (40, 41, 50), which have  
337 been shown to be relevant in CA fields as well (22). All this suggests that the hippocampus and  
338 DG in particular, might convey information through multiple simultaneously relevant timescales.

339         Most of our results are reported at a 10 ms resolution, which corresponds approximately  
340 to the spike jitter in GCs (**S2 Fig**) as well as their time constant and the gamma rhythm. This  
341 choice of temporal resolution is similar to a recent computational study of pattern separation

342 within a DG model, which used a 20 ms resolution on short spiketrains (30 ms inputs, 200 ms  
343 outputs) (17). Furthermore, we found that GCs perform pattern separation both at the millisecond  
344 timescale, through orthogonalization or by rearranging spike times, and at the second timescale  
345 by varying their firing rate, with a smooth transition around 100 ms (**Fig 4**). Therefore, our work  
346 demonstrates for the first time that multiple codes for pattern separation coexist within DG at  
347 simultaneously relevant timescales, consistent with a potential multiplexing of signals in the  
348 hippocampus.

349

### 350 **Computational and physiological mechanisms of temporal pattern separation**

351 The mechanisms supporting pattern separation within DG had so far never been experimentally  
352 investigated. The orthogonalization of sequentially presented input patterns can in theory be  
353 explained by: 1) adaptive mechanisms, involving learning and recognition of input patterns,  
354 comparison with previously stored ones and the pruning out of common features, 2) non-  
355 adaptive (intrinsic) mechanisms, 3) or both (51). First, concerning adaptive mechanisms, it has  
356 been suggested that Hebbian learning could enhance population pattern separation in the DG  
357 (52), but computational models testing different forms of synaptic learning found that it would  
358 actually impair this type of pattern separation (4, 19). As for temporal pattern separation, our  
359 data show that it hardly benefits from the repetition of input patterns (**Fig 5**). Second, we offer  
360 indirect evidence that non-adaptive decorrelation processes support temporal pattern separation  
361 because output patterns are always decorrelated to the same proportion (**Fig 2E**), a feat that a  
362 simple random process can achieve (**Fig S4D**), suggesting that input patterns do not need to be  
363 recognized. Third, adaptive and non-adaptive mechanisms are not mutually exclusive: previous  
364 learning over days, during the neuron maturation process, could tune single GCs only to specific



365 input patterns, allowing rapid pattern separation (53). Indeed, a computational study suggested  
366 that adaptive networks can mature to perform a fast, non-adaptive orthogonalization of the  
367 population activity by the decorrelation between individual information channels (54).

368 Adaptive or not, what is the biological source of the temporal decorrelation we observed?  
369 Synaptic and intrinsic neural noises are obvious candidates, but simple randomness was not  
370 sufficient to reproduce our results (**Fig 6** and **S4 Fig**). More complex and realistic noisy  
371 processes including synaptic short-term plasticity as well as inhibition might have a role.  
372 However we showed that FS, which provide both feedforward and feedback inhibition to the  
373 soma of GCs (34, 35), exhibit poor ability to separate spiketrains. On the other hand, their ability  
374 to relay information reliably (35) (**Fig 8** and **S6 Fig**) and to precisely control spike timing in  
375 target neurons (35) might actually provide a mechanism that counteracts noisiness in GCs,  
376 increasing the fidelity of information transmission to CA3 (while still allowing effective  
377 spiketrain separation in GCs).

378

### 379 **The role of sweep-to-sweep variability**

380 Because the brain needs to be able to recognize when situations are exactly the same, our finding  
381 that pattern separation occurs even when the same input pattern is repeated (**Fig 6A**) might seem  
382 counter-intuitive at first. However, in theory, the separation and the recognition functions do not  
383 have to be supported by the same network. The Hebb-Marr framework actually hypothesizes that  
384 CA3 is able to recall the original pattern from a noisy input from DG. Even though most  
385 computational models that tested the effect of repetition were consistent with the intuitive view  
386 (4, 17), this was likely because they used deterministic neurons. A model considering variability  
387 across GCs and a probabilistic spiking behavior had results similar to ours (32).

388           In the cortex, the well-known variability of single neuron activity between trials is often  
389 supposed to be "averaged out" at the population level so that the output of the population is  
390 reliable (30). It is thus conceivable that considering an ensemble of GCs would increase the  
391 signal-to-noise ratio. In fact, when we average out the sweep-to-sweep variability, GCs exhibit  
392 pattern separation for highly similar patterns but almost no separation for identical ones (**Fig 7D-**  
393 **E**).

394           However, this variability is not necessarily meaningless (30). Our results suggest it might  
395 be a mechanism amplifying pattern separation (**Fig 7**). The variability might even be just  
396 apparent, if we consider that when the same input is repeated it is at different points in time: each  
397 repetition could be considered as a different event that need to be encoded slightly differently.  
398 The role of single GCs could thus be to meaningfully add some noise to transform input  
399 spiketrains so that cortical information about an event is stored in the hippocampus with a unique  
400 random time-stamp, consistent with the index theory of episodic memory (55).

401

## 402 **The computational importance of temporal pattern separation in single cells to the** 403 **population level**

404           Although more work is needed to test whether the DG is a pattern separator at the population  
405 level, the discovery of temporal pattern separation in single GCs has strong implications for  
406 population dynamics. The fact that, in response to the same patterns, single GCs rearrange their  
407 spikes differently from sweep to sweep (**Fig 6A**) and from cell to cell (**Fig 9A**) may enforce very  
408 small neuronal assemblies in the DG (23). In other words, these processes may insure that a  
409 minimal number of output neurons are active at the same time: such sparsity in active neuronal

410 population is known, from computational studies, to be critical for efficient population pattern  
411 separation (4, 18, 56).

412

## 413 **Materials and Methods**

414

### 415 **Animals and dissection**

416 Horizontal slices (57) of the ventral and intermediate hippocampus (400  $\mu$ m) were prepared from  
417 the brains of C57BL/6 male mice 15 – 25 days old (Harlan). All procedures were approved by  
418 the University of Wisconsin Institutional Animal Care and Use Committee. Mice were  
419 anesthetized with isoflurane, decapitated, and the brain was removed quickly and placed in ice-  
420 cold cutting solution containing (in mM) 83 NaCl, 26 NaHCO<sub>3</sub>, 2.5 KCl, 1 NaH<sub>2</sub>PO<sub>4</sub>, 0.5 CaCl<sub>2</sub>,  
421 3.3 MgCl<sub>2</sub>, 22 D-Glucose and 72 Sucrose, bubbled with 95% O<sub>2</sub> and 5% CO<sub>2</sub>. Horizontal slices  
422 were cut using a vibratome (Leica VT1000S) and placed in an incubation chamber in standard  
423 artificial cerebrospinal fluid (aCSF) containing (in mM) 125 NaCl, 25 NaHCO<sub>3</sub>, 2.5 KCl, 1.25  
424 NaH<sub>2</sub>PO<sub>4</sub>, 2 CaCl<sub>2</sub>, 1 MgCl<sub>2</sub>, and 25 D-Glucose (or in a 50/50 mix of cutting solution and  
425 standard aCSF) at 35° C, for 15-30 minutes after dissection. Slices were stored in the incubation  
426 chamber at room temperature for at least 30 minutes before being used for recordings.

427

### 428 **Electrophysiology**

429 All recordings were done in aCSF. Whole cell patch-clamp recordings were made using an  
430 upright microscope (Axioskop FS2, Zeiss, Oberkochen, Germany) with infra-red differential  
431 interference contrast optics. Patch pipettes pulled from thin-walled borosilicate glass (World  
432 Precision Instruments, Sarasota, FL) had a resistance of 3-5 M $\Omega$  when filled with intracellular

433 solution containing (in mM) 140 K-gluconate, 10 EGTA, 10 HEPES, 20 phosphocreatine, 2  
434  $Mg_2ATP$ , 0.3 NaGTP (pH 7.3, 310 mOsm). Recordings were done at physiological temperature  
435 (33-35 °C) using one or two Axopatch 200B amplifiers (Axon Instruments, Foster City, CA),  
436 filtered at 5 kHz using a 4-pole Bessel filter and digitized at 10 kHz using a Digidata 1320A  
437 analog-digital interface (Axon Instruments). Data were acquired to a Macintosh G4 (Apple  
438 Computer, Cupertino, CA) using Axograph X v1.0.7 (AxographX.com). Stimulation pipettes  
439 were pulled from double barrel borosilicate theta-glass (~10  $\mu m$  tip diameter, Harvard  
440 Apparatus, Edenbridge, U.K.) and filled with ACSF or a 1M NaCl solution and connected to a  
441 constant current stimulus isolator used to generate 0.1-10 mA pulses, 100 microseconds in  
442 duration. GCs used for analysis ( $n = 28$ ) were stable across a whole recording session as judged  
443 by monitoring of series resistance and resting potential, with the following characteristics: series  
444 resistance ( $R_s$ ):  $6.65 \pm 0.68 M\Omega$ ; resting potential ( $V_{rest}$ ):  $-69.3 \pm 1.3 mV$  (min = -80 mV, max = -  
445 51 mV); input resistance ( $R_i$ ):  $171 \pm 16 M\Omega$  (min = 81  $M\Omega$ , max = 325  $M\Omega$ ) and capacitance  
446 ( $C_m$ ):  $23 \pm 2 pF$  (min = 12 pF, max = 65 pF). Fast-spiking (FS) interneurons ( $n = 4$ ) were  
447 identified as neurons with large somata at the hilus-granule cell layer border and a high firing  
448 rate response during large depolarizing current steps (34, 58) (Fig. 7). They had the following  
449 characteristics:  $R_s$ :  $7.2 \pm 1.2 M\Omega$ ;  $V_{rest}$ :  $-66.7 \pm 3.5 mV$  (min = -72 mV, max = -55 mV);  $R_i$ :  $59 \pm$   
450  $10 M\Omega$  (min = 41  $M\Omega$ , max = 92  $M\Omega$ ) and  $C_m$ :  $19 \pm 3 pF$  (min = 13 pF, max = 30 pF).

451

## 452 **Pattern separation experiments**

453 Input patterns were 2 second long traces of impulses simulating cortical spiketrains, with  
454 interspike intervals following a Poisson distribution of mean frequency ~10 Hz ( $11.9 \pm 0.7$  Hz,  
455 min = 9.6 Hz, max = 14.5 Hz). Firing rates were chosen to be consistent with the frequency of

456 EPSCs recorded in GCs of behaving mice (46), and are known to promote a high probability of  
457 spiking in GCs in slices (34, 59). Eleven sets of five input trains were designed so that the 5  
458 trains of each set would have a prespecified average correlation coefficient  $R_{\text{input}}$  when using a  
459 binning window  $\tau_w$  of 10 ms. The relative standard error of the input set similarity was on  
460 average 4% of the mean for  $R_{\text{input}}$  at  $\tau_w = 10$  ms, and it was similarly constrained for other time  
461 resolutions and similarity metrics. Five sets were designed with an algorithm developed in-house  
462 (at  $\tau_w = 10$  ms,  $R_{\text{input}} = 0.88, 0.84, 0.73, 0.65, 0.56$ ) and six other sets were designed using the  
463 algorithm of Macke and colleagues (60) (at  $\tau_w = 10$  ms,  $R_{\text{input}} = 1.00, 0.95, 0.76, 0.48, 0.25,$   
464  $0.11$ ). Because results did not qualitatively differ when considering data obtained from the two  
465 groups of input sets, we pooled them together for our analysis.

466         The spiking response of a DG neuron was recorded in whole-cell mode while stimuli  
467 were delivered to the outer molecular layer (OML). Stimulus current intensity and location were  
468 set so that the recorded neuron spiked occasionally in response to electrical impulses and the  
469 stimulation electrode was at least 100  $\mu\text{m}$  away from the expected location of the dendrites of the  
470 recorded neuron. Once stimulation parameters were set, a pattern separation protocol was run. It  
471 consisted of a sequence of the five different input spiketrains, delivered one after the other  
472 separated by 4 s of relaxation, repeated ten times. The ten repetitions of the sequence of five  
473 patterns were implemented to take into account any potential variability in the output, and the  
474 non-random sequential scheme was used to avoid repeating the same input spiketrain close in  
475 time. Each protocol yielded a recording set consisting of fifty output spiketrains, each associated  
476 with one of the five different input spiketrains (**Fig 1C**).  $V_{\text{rest}}$  was maintained around -70mV  
477 during recordings, consistent with the  $V_{\text{rest}}$  of mature GCs recorded in behaving mice (46). The  
478 output spiking frequency was variable ( $6.3 \pm 0.3\text{Hz}$ , see **S5B Fig**) but consistent with sparse

479 activity generally observed in GCs *in vivo* (11, 12, 46, 47, 61) and in slices under conditions of  
480 drive comparable to what was used here (62, 63).

481

## 482 **Similarity metrics**

483 Similarity between spiketrains was assessed in four ways: 1) with the Pearson's correlation  
484 coefficient (R), 2) with the normalized dot product (NDP), 3) with the scaling factor (SF) and 4)  
485 with a distance metric called SPIKE specifically designed to assess the dissimilarity between two  
486 spiketrains (29). The SPIKE-metric is a binless metric based on spike times, whereas R, NDP  
487 and SF are based on the number of spikes occurring in time bins of prespecified durations (e.g.  
488  $\tau_w = 10$  ms).

489 For R, two spiketrains X and Y of the same duration, divided into N time bins of size  $\tau_w$   
490 are seen as variables, with  $X_i$  and  $Y_i$  the observations, i.e. the respective numbers of spikes in bin  
491 i for each spiketrain. R assesses the similarity between X and Y by measuring the goodness of fit  
492 of a linear regression to the distribution of points  $(X_i, Y_i)$ : when R is close to 1 spiketrains are  
493 similar, close to 0 they are dissimilar and close to -1 they are anticorrelated (**Fig 3A-B**). R was  
494 computed with the following equation, where *cov* is the covariance,  $\sigma$  is the standard deviation  
495 and  $\bar{X}$  and  $\bar{Y}$  are the means of X and Y):

496

$$R = \frac{\text{cov}(X, Y)}{\sigma_X \cdot \sigma_Y} = \frac{\sum_{i=1}^N (X_i - \bar{X}) \cdot (Y_i - \bar{Y})}{\sqrt{\sum_{i=1}^N (X_i - \bar{X})^2} \cdot \sqrt{\sum_{i=1}^N (Y_i - \bar{Y})^2}}$$

497

498 NDP and SF are similarity metrics explicitly considering spiketrains as vectors. They,  
499 like R, require arbitrarily dividing spiketrains into time bins, which are considered dimensions of

500 an N-dimensional space where N is the number of bins. For two binned spiketrains X and Y,  
501 NDP is the cosine of the angle  $\theta$  between the two vectors: 0 when they are perfectly orthogonal,  
502 1 when they are collinear (**Fig 3A, C**). The NDP is defined as the scalar product of X and Y  
503 divided by their norms, and was computed with the following equation (where  $X_i$  and  $Y_i$  are the  
504 coordinates of X and Y, measuring the number of spikes in bin  $i$ ):

505

$$\text{NDP} = \cos(\theta) = \frac{\sum_{i=1}^N X_i \cdot Y_i}{\sqrt{\sum_{i=1}^N X_i^2} \cdot \sqrt{\sum_{i=1}^N Y_i^2}}$$

506

507 SF, on the other hand, quantifies the difference of length between the two vectors X and  
508 Y, or, in other words, the variation in the binwise firing rate between two spiketrains. We have  
509 defined it as the ratio between the norms of each vector, the smaller norm always divided by the  
510 bigger one to have SF values ranging from 0 to 1. When norms  $\|X\|$ ,  $\|Y\|$  or both were 0 (i.e.  
511 spiketrains without spikes), SF was excluded from further analysis. SF = 1 means X and Y are  
512 identical in terms of binwise spike number. The closer to 0 SF is, the more dissimilar are the  
513 binwise firing rates (**Fig 3A, C**). SF was computed with the following equation (where  $0 < \|X\| \leq$   
514  $\|Y\|$ ):

515

$$SF = \frac{\sqrt{\sum_{i=1}^N X_i^2}}{\sqrt{\sum_{i=1}^N Y_i^2}}$$

516

517 Comparing the three equations above, the relationships between R, NDP and SF are not  
518 trivial and not linear. Note that R is actually an NDP, but of vectors centered to their respective

519 mean, which does not conserve the angular relationship between X and Y. This centering also  
520 makes R a similarity metric intrinsically independent of differences in mean firing rates between  
521 X and Y (43, 64), as opposed to NDP and SF. (NB: this does not prevent a physiological  
522 dependency, as shown by de la Rocha and colleagues (2007) and our results in **S5B Fig**). To  
523 further evaluate the relationship between R, NDP and SF, we generated a set of 1012 spike  
524 rasters (1000 were random, 12 were specific cases) between which we computed the similarity  
525 with the three metrics above. Each raster was made of six bins, each bin containing 0, 1 or 2  
526 spikes (drawn from a uniform distribution for the randomly generated group). This analysis  
527 confirmed that the three metrics are not equivalent and provides an intuition on what each metric  
528 represents (**S1D Fig**).

529 As explained above, R, NDP and SF are binned measures, with  $\tau_w$  the specified temporal  
530 resolution. In other words, in all the equations above,  $X_i$  and  $Y_i$  are functions of  $\tau_w$  and the values  
531 of the respective similarity metrics are dependent on  $\tau_w$  as well. In **Fig 4**, we evaluated the  
532 influence of  $\tau_w$  on the results by varying it between 5 ms and 2000 ms. Note that because our  
533 spiketrains are 2 seconds long, using  $\tau_w = 2000$  ms means the spiketrains can be seen as variables  
534 with only one observation, or as unidimensional vectors that can only vary by their norm. In this  
535 case, R is meaningless, NDP is necessarily 1, which indicates collinearity, and SF correctly  
536 assesses the variation in the overall firing rate between the two spiketrains. Our analysis  
537 therefore explores a wide range of coding strategies between a temporal code with 5 ms  
538 resolution and a pure rate code.

539 Being binned metrics, R, NDP and SF also have the drawback of considering all  $X_i$  (i.e.  
540 bins) as independent observations, which may not be a realistic assumption. The binless SPIKE  
541 similarity metric avoids this limitation. SPIKE also differs from the other measures by not



542 assuming that spiketrains are related linearly, or that they belong to a Euclidean space (65). To  
543 compute SPIKE, we used the Matlab toolbox provided at  
544 [www.fi.isc.cnr.it/users/thomas.kreuz/sourcecode.html](http://www.fi.isc.cnr.it/users/thomas.kreuz/sourcecode.html) which computes the SPIKE-distance (called D(t)  
545 in our study and S(t) in the original paper: see equation 19) (29). The SPIKE similarity was  
546 computed as:  $SPIKE = 1 - \frac{1}{T} \int_0^T D(t) dt$ , where T is the duration of the spiketrain. Because D(t)  
547 ranges from 0 to 1, SPIKE is thus also between 0 and 1, like NDP and SF. When SPIKE is equal  
548 to 1, spiketrains have exactly the same spike times, i.e. they are synchronous (n.b. in our  
549 experiments, spiketrains were not simultaneously recorded, but we use "synchronous" in the  
550 sense of spiketrains aligned to the start of each 2 s sweep). Note that SPIKE has a large dynamic  
551 range (i.e. sensitivity over large differences of spiketimes), and, as a result, realistic spiketrains  
552 like in our input sets rarely have a SPIKE similarity lower than 0.5 (29) (**Fig 4C**).

553

$-1 \leq R \leq 1$
$0 \leq NDP \leq 1$
$0 < SF \leq 1$
$0 \leq SPIKE\text{-similarity} \leq 1$ ; but $\geq 0.5$ in most cases

554

555 **Noise parameters.** We define the spike-wise neural noise as the delay of an output spike after an  
556 input spike, its average jitter and its spiking reliability (SR, below) which is linked to the rate of  
557 failure to spike after an input spike. To assess these parameters, we computed the cross-  
558 occurrence between input spikes and output spikes in a [-15 ms, 50ms] interval with 1 ms bins,  
559 for each recording set. The resulting histogram of counts of output spikes occurring in the  
560 vicinity of an input spike was fitted with a Gaussian distribution  $N(\mu, \sigma, \text{baseline})$ , where  $\mu$  is the

561 mean delay of an output spike and  $\sigma$  is the jitter of this delay. The baseline corresponds to the  
562 background firing, occurring by chance or caused by neighboring inputs. After subtracting the  
563 baseline and extracting the probability of spiking by dividing the counts of output spikes by the  
564 total number of input spikes, we defined the *spiking reliability* (SR) as the sum of probabilities of  
565 an output spike in the predefined time interval around an input spike (**Fig 6B** and **S2A Fig**).

566  
567 **Simulated and shuffled data.** To assess the role of spike-wise neural noise in pattern separation,  
568 we generated two data sets. First, we simulated output spiketrains in response to our 11 input sets  
569 (10 simulated output sets of 50 synthetic spiketrains per input set). This simulation was entirely  
570 based on the average spike-wise noise parameters computed from the real GC recordings (see  
571 above): the matrix of input spike times was replicated ten times, and for each of the 50 resulting  
572 sweeps, spikes were deleted randomly following a binomial distribution  $B(\text{Number of spikes}, 1-$   
573  $\text{mean SR} = 1-0.42)$ . A random delay, sampled from a Gaussian distribution  $N(\mu, \sigma)$ , was added to  
574 each resulting spike times, with  $\mu$  and  $\sigma$  being respectively the mean delay and mean jitter in the  
575 original recordings. The noise statistics of the resulting simulated data set is shown in **S2C Fig**.

576  
577 Second, we created a surrogate data set by randomly shuffling the output spikes of the  
578 original GC recordings: the delay of each spike was conserved but it was relocated to follow a  
579 randomly selected input spike in the same input train (from a uniform distribution). This strategy  
580 yielded a data set with noise statistics closer to the original data (**S2D Fig**).

580

## 581 **Software and statistics**

582 Data analysis was performed using custom-written routines in Matlab (Mathworks, Natick, MA,  
583 USA), including functions from toolboxes cited above. Sample sizes were chosen based on the

584 literature and estimations of the variance and effect size from preliminary data. All values are  
585 reported as mean  $\pm$  S.E.M. unless otherwise noted. The one-sample Kolmogorov-Smirnov test  
586 was used to verify the normality of data distributions. Parametric or non-parametric statistical  
587 tests (see figure legends) were appropriately used to assess significance ( $p$ -value  $< 0.05$ ).  
588 Assumptions on equal variances between groups were avoided when necessary. All T and U tests  
589 were two-tailed. To determine whether two distributions of data points are significantly different  
590 (e.g.  $R_{\text{output}}$  as a function of  $R_{\text{input}}$ , for GC compared to FS, see **Fig. 5, 6, S4, 7, S5**), we performed  
591 a regression (linear or parabolic) on the two data sets as well as on the combined data set, and  
592 assessed significance via an F-test comparing the goodness of fits (66). Because  $R_{\text{input}}$  can also be  
593 considered as a categorical variable, we performed a two-way ANOVA before using post-hoc  
594 tests correcting for multiple comparisons in order to determine at which  $R_{\text{input}}$  groups two  
595 conditions were significantly different.

596

## 597 **References**

- 598 1. McNaughton BL, Morris RGM. Hippocampal synaptic enhancement and information  
599 storage within a distributed memory system. *Trends in Neuroscience*. 1987;10(10):408-15.
- 600 2. Treves A, Tashiro A, Witter MP, Moser EI. What is the mammalian dentate gyrus good  
601 for? *Neuroscience*. 2008 Jul 17;154(4):1155-72. PubMed PMID: 18554812. Epub 2008/06/17.  
602 eng.
- 603 3. Rolls ET. A computational theory of episodic memory formation in the hippocampus.  
604 *Behavioural brain research*. 2010 Dec 31;215(2):180-96. PubMed PMID: 20307583.

- 605 4. O'Reilly RC, McClelland JL. Hippocampal conjunctive encoding, storage, and recall:  
606 avoiding a trade-off. *Hippocampus*. 1994 Dec;4(6):661-82. PubMed PMID: 7704110. Epub  
607 1994/12/01. eng.
- 608 5. Santoro A. Reassessing pattern separation in the dentate gyrus. *Frontiers in behavioral*  
609 *neuroscience*. 2013;7:96. PubMed PMID: 23908611. Pubmed Central PMCID: 3726960.
- 610 6. Amaral DG, Scharfman HE, Lavenex P. The dentate gyrus: fundamental neuroanatomical  
611 organization (dentate gyrus for dummies). 2007;163:3-790.
- 612 7. McHugh TJ, Jones MW, Quinn JJ, Balthasar N, Coppari R, Elmquist JK, et al. Dentate  
613 gyrus NMDA receptors mediate rapid pattern separation in the hippocampal network. *Science*.  
614 2007 Jul 6;317(5834):94-9. PubMed PMID: 17556551.
- 615 8. Kesner RP, Rolls ET. A computational theory of hippocampal function, and tests of the  
616 theory: new developments. *Neuroscience and biobehavioral reviews*. 2015 Jan;48:92-147.  
617 PubMed PMID: 25446947. Epub 2014/12/03. Eng.
- 618 9. Kesner RP, Kirk RA, Yu Z, Polansky C, Musso ND. Dentate gyrus supports slope  
619 recognition memory, shades of grey-context pattern separation and recognition memory, and  
620 CA3 supports pattern completion for object memory. *Neurobiology of learning and memory*.  
621 2016 Mar;129:29-37. PubMed PMID: 26318932. Epub 2015/09/01. eng.
- 622 10. Baker S, Vieweg P, Gao F, Gilboa A, Wolbers T, Black SE, et al. The Human Dentate  
623 Gyrus Plays a Necessary Role in Discriminating New Memories. *Current biology : CB*. 2016 Sep  
624 21. PubMed PMID: 27666968. Epub 2016/09/27. Eng.
- 625 11. Leutgeb JK, Leutgeb S, Moser MB, Moser EI. Pattern separation in the dentate gyrus and  
626 CA3 of the hippocampus. *Science*. 2007 Feb 16;315(5814):961-6. PubMed PMID: 17303747.

- 627 12. Neunuebel JP, Knierim JJ. CA3 retrieves coherent representations from degraded input:  
628 direct evidence for CA3 pattern completion and dentate gyrus pattern separation. *Neuron*. 2014  
629 Jan 22;81(2):416-27. PubMed PMID: 24462102. Pubmed Central PMCID: 3904133.
- 630 13. Deng W, Mayford M, Gage FH. Selection of distinct populations of dentate granule cells  
631 in response to inputs as a mechanism for pattern separation in mice. *eLife*. 2013;2:e00312.  
632 PubMed PMID: 23538967. Pubmed Central PMCID: PMC3602954. Epub 2013/03/30. eng.
- 633 14. Marrone DF, Adams AA, Satvat E. Increased pattern separation in the aged fascia  
634 dentata. *Neurobiology of aging*. 2011 Dec;32(12):2317 e23-32. PubMed PMID: 20447731. Epub  
635 2010/05/08. eng.
- 636 15. Nakazawa K. Dentate Mossy Cell and Pattern Separation. *Neuron*. 2017;93(3):465-7.
- 637 16. Myers CE, Scharfman HE. A role for hilar cells in pattern separation in the dentate gyrus:  
638 a computational approach. *Hippocampus*. 2009 Apr;19(4):321-37. PubMed PMID: 18958849.  
639 Pubmed Central PMCID: 2723776.
- 640 17. Yim MY, Hanuschkin A, Wolfart J. Intrinsic rescaling of granule cells restores pattern  
641 separation ability of a dentate gyrus network model during epileptic hyperexcitability.  
642 *Hippocampus*. 2014 Oct 1. PubMed PMID: 25269417. Epub 2014/10/02. Eng.
- 643 18. Chavlis S, Petrantonakis PC, Poirazi P. Dendrites of dentate gyrus granule cells  
644 contribute to pattern separation by controlling sparsity. *Hippocampus*. 2017.
- 645 19. Neher T, Cheng S, Wiskott L. Memory storage fidelity in the hippocampal circuit: the  
646 role of subregions and input statistics. *PLoS computational biology*. 2015 May;11(5):e1004250.  
647 PubMed PMID: 25954996. Pubmed Central PMCID: PMC4425359. Epub 2015/05/09. eng.
- 648 20. Chawla MK, Guzowski JF, Ramirez-Amaya V, Lipa P, Hoffman KL, Marriott LK, et al.  
649 Sparse, environmentally selective expression of Arc RNA in the upper blade of the rodent fascia

- 650 dentata by brief spatial experience. *Hippocampus*. 2005;15(5):579-86. PubMed PMID:  
651 15920719. Epub 2005/05/28. eng.
- 652 21. Ramirez S, Liu X, Lin PA, Suh J, Pignatelli M, Redondo RL, et al. Creating a false  
653 memory in the hippocampus. *Science*. 2013 Jul 26;341(6144):387-91. PubMed PMID:  
654 23888038.
- 655 22. Kelemen E, Fenton AA. Coordinating different representations in the hippocampus.  
656 *Neurobiology of learning and memory*. 2016 Mar;129:50-9. PubMed PMID: 26748023. Epub  
657 2016/01/10. eng.
- 658 23. Buzsaki G. Neural syntax: cell assemblies, synapsembles, and readers. *Neuron*. 2010 Nov  
659 4;68(3):362-85. PubMed PMID: 21040841. Pubmed Central PMCID: 3005627.
- 660 24. Eichenbaum H. Time cells in the hippocampus: a new dimension for mapping memories.  
661 *Nature reviews Neuroscience*. 2014 Nov;15(11):732-44. PubMed PMID: 25269553. Pubmed  
662 Central PMCID: PMC4348090. Epub 2014/10/02. eng.
- 663 25. Rieke F. WW, de Ruyter van Steveninck R., Bialek W. *Spikes: Exploring the Neural*  
664 *Code*. PRESS TM, editor: A Bradford Book; 1999.
- 665 26. VanRullen R, Guyonneau R, Thorpe SJ. Spike times make sense. *Trends in*  
666 *neurosciences*. 2005 Jan;28(1):1-4. PubMed PMID: 15626490. Epub 2005/01/01. eng.
- 667 27. Gutig R. To spike, or when to spike? *Current opinion in neurobiology*. 2014 Apr;25:134-  
668 9. PubMed PMID: 24468508. Epub 2014/01/29. eng.
- 669 28. Hopfield JJ. Neural networks and physical systems with emergent collective  
670 computational abilities. *Proceedings of the National Academy of Sciences of the United States of*  
671 *America*. 1982 Apr;79(8):2554-8. PubMed PMID: 6953413. Pubmed Central PMCID:  
672 PMC346238. Epub 1982/04/01. eng.

- 673 29. Kreuz T, Chicharro D, Houghton C, Andrzejak RG, Mormann F. Monitoring spike train  
674 synchrony. *Journal of neurophysiology*. 2013 Mar;109(5):1457-72. PubMed PMID: 23221419.  
675 Epub 2012/12/12. eng.
- 676 30. Faisal AA, Selen LP, Wolpert DM. Noise in the nervous system. *Nature reviews*  
677 *Neuroscience*. 2008 Apr;9(4):292-303. PubMed PMID: 18319728. Pubmed Central PMCID:  
678 PMC2631351. Epub 2008/03/06. eng.
- 679 31. Dobrunz LE, Stevens CF. Response of hippocampal synapses to natural stimulation  
680 patterns. *Neuron*. 1999 Jan;22(1):157-66. PubMed PMID: 10027298. Epub 1999/02/23. eng.
- 681 32. Aimone JB, Wiles J, Gage FH. Computational influence of adult neurogenesis on  
682 memory encoding. *Neuron*. 2009 Jan 29;61(2):187-202. PubMed PMID: 19186162. Pubmed  
683 Central PMCID: 2670434.
- 684 33. Savanthrapadian S, Meyer T, Elgueta C, Booker SA, Vida I, Bartos M. Synaptic  
685 Properties of SOM- and CCK-Expressing Cells in Dentate Gyrus Interneuron Networks. *The*  
686 *Journal of neuroscience : the official journal of the Society for Neuroscience*. 2014 Jun  
687 11;34(24):8197-209. PubMed PMID: 24920624.
- 688 34. Ewell LA, Jones MV. Frequency-tuned distribution of inhibition in the dentate gyrus.  
689 *The Journal of neuroscience : the official journal of the Society for Neuroscience*. 2010 Sep  
690 22;30(38):12597-607. PubMed PMID: 20861366. Epub 2010/09/24. eng.
- 691 35. Hu H, Gan J, Jonas P. Interneurons. Fast-spiking, parvalbumin(+) GABAergic  
692 interneurons: from cellular design to microcircuit function. *Science*. 2014 Aug  
693 1;345(6196):1255263. PubMed PMID: 25082707.
- 694 36. Neunuebel JP, Knierim JJ. Spatial firing correlates of physiologically distinct cell types  
695 of the rat dentate gyrus. *The Journal of neuroscience : the official journal of the Society for*

- 696 Neuroscience. 2012 Mar 14;32(11):3848-58. PubMed PMID: 22423105. Pubmed Central  
697 PMCID: 3321836.
- 698 37. Senzai Y, Buzsáki G. Physiological properties and behavioral correlates of hippocampal  
699 granule cells and mossy cells. *Neuron*. 2017;93(3):691-704. e5.
- 700 38. GoodSmith D, Chen X, Wang C, Kim SH, Song H, Burgalossi A, et al. Spatial  
701 representations of granule cells and mossy cells of the dentate gyrus. *Neuron*. 2017;93(3):677-  
702 90. e5.
- 703 39. Danielson NB, Turi GF, Ladow M, Chavlis S, Petrantonakis PC, Poirazi P, et al. In Vivo  
704 Imaging of Dentate Gyrus Mossy Cells in Behaving Mice. *Neuron*. 2017;93(3):552-9. e4.
- 705 40. Hyde RA, Strowbridge BW. Mnemonic representations of transient stimuli and temporal  
706 sequences in the rodent hippocampus in vitro. *Nature neuroscience*. 2012 Oct;15(10):1430-8.  
707 PubMed PMID: 22960934. Pubmed Central PMCID: 3614351.
- 708 41. Zylberberg J, Hyde RA, Strowbridge BW. Dynamics of robust pattern separability in the  
709 hippocampal dentate gyrus. *Hippocampus*. 2016 May;26(5):623-32. PubMed PMID: 26482936.  
710 Epub 2015/10/21. eng.
- 711 42. Chavlis S, Poirazi P. Pattern separation in the hippocampus through the eyes of  
712 computational modeling. *Synapse (New York, NY)*. 2017 Mar 18. PubMed PMID: 28316111.  
713 Epub 2017/03/21. eng.
- 714 43. Cutts CS, Eglen SJ. Detecting pairwise correlations in spike trains: an objective  
715 comparison of methods and application to the study of retinal waves. *The Journal of*  
716 *neuroscience : the official journal of the Society for Neuroscience*. 2014 Oct 22;34(43):14288-  
717 303. PubMed PMID: 25339742. Pubmed Central PMCID: PMC4205553. Epub 2014/10/24. eng.



- 718 44. Lyttle D, Fellous JM. A new similarity measure for spike trains: sensitivity to bursts and  
719 periods of inhibition. *Journal of neuroscience methods*. 2011 Aug 15;199(2):296-309. PubMed  
720 PMID: 21600921. Pubmed Central PMCID: PMC4120777. Epub 2011/05/24. eng.
- 721 45. Kreuz T. Measures of spike train synchrony. *Scholarpedia* [Internet]. 2011; 6(10).  
722 Available from: [http://www.scholarpedia.org/article/Measures\\_of\\_spike\\_train\\_synchrony](http://www.scholarpedia.org/article/Measures_of_spike_train_synchrony).
- 723 46. Pernía-Andrade Alejandro J, Jonas P. Theta-Gamma-Modulated Synaptic Currents in  
724 Hippocampal Granule Cells In Vivo Define a Mechanism for Network Oscillations. *Neuron*.  
725 2014;81(1):140-52.
- 726 47. Diamantaki M, Frey M, Berens P, Preston-Ferrer P, Burgalossi A. Sparse activity of  
727 identified dentate granule cells during spatial exploration. *eLife*. 2016 Oct 03;5. PubMed PMID:  
728 27692065. Epub 2016/10/04. Eng.
- 729 48. Lisman JE, Jensen O. The theta-gamma neural code. *Neuron*. 2013 Mar 20;77(6):1002-  
730 16. PubMed PMID: 23522038. Pubmed Central PMCID: 3648857.
- 731 49. Wikenheiser AM, Redish AD. Decoding the cognitive map: ensemble hippocampal  
732 sequences and decision making. *Current opinion in neurobiology*. 2015;32:8-15.
- 733 50. Larimer P, Strowbridge BW. Representing information in cell assemblies: persistent  
734 activity mediated by semilunar granule cells. *Nature neuroscience*. 2010 Feb;13(2):213-22.  
735 PubMed PMID: 20037579. Pubmed Central PMCID: 2840722.
- 736 51. Friedrich RW, Wiechert MT. Neuronal circuits and computations: pattern decorrelation  
737 in the olfactory bulb. *FEBS letters*. 2014 Aug 1;588(15):2504-13. PubMed PMID: 24911205.  
738 Epub 2014/06/10. eng.
- 739 52. Fontanari J, Rolls E, Costa DF. A model of the operation of the hippocampus and  
740 entorhinal cortex in memory. *International Journal of Neural Systems*. 1995;6(1):51-70.

- 741 53. Aimone JB, Deng W, Gage FH. Resolving new memories: a critical look at the dentate  
742 gyrus, adult neurogenesis, and pattern separation. *Neuron*. 2011 May 26;70(4):589-96. PubMed  
743 PMID: 21609818. Pubmed Central PMCID: PMC3240575. Epub 2011/05/26. eng.
- 744 54. Wick SD, Wiechert MT, Friedrich RW, Riecke H. Pattern orthogonalization via channel  
745 decorrelation by adaptive networks. *Journal of computational neuroscience*. 2010 Feb;28(1):29-  
746 45. PubMed PMID: 19714457. Epub 2009/08/29. eng.
- 747 55. Teyler TJ, Rudy JW. The hippocampal indexing theory and episodic memory: updating  
748 the index. *Hippocampus*. 2007;17(12):1158-69. PubMed PMID: 17696170. Epub 2007/08/19.  
749 eng.
- 750 56. Severa W, Parekh O, James CD, Aimone JB. A Combinatorial Model for Dentate Gyrus  
751 Sparse Coding. *Neural computation*. 2016 Oct 20:1-24. PubMed PMID: 27764589. Epub  
752 2016/10/21. Eng.
- 753 57. Bischofberger J, Engel D, Li L, Geiger JR, Jonas P. Patch-clamp recording from mossy  
754 fiber terminals in hippocampal slices. *Nature protocols*. 2006;1(4):2075-81. PubMed PMID:  
755 17487197. Epub 2007/05/10. eng.
- 756 58. Harney SC, Jones MV. Pre- and postsynaptic properties of somatic and dendritic  
757 inhibition in dentate gyrus. *Neuropharmacology*. 2002 Sep;43(4):584-94. PubMed PMID:  
758 12367604. Epub 2002/10/09. eng.
- 759 59. Andersen P, Holmqvist B, Voorhoeve PE. Excitatory synapses on hippocampal apical  
760 dendrites activated by entorhinal stimulation. *Acta physiologica Scandinavica*. 1966  
761 Apr;66(4):461-72. PubMed PMID: 5927272. Epub 1966/04/01. eng.

- 762 60. Macke JH, Berens P, Ecker AS, Tolias AS, Bethge M. Generating spike trains with  
763 specified correlation coefficients. *Neural computation*. 2009 Feb;21(2):397-423. PubMed PMID:  
764 19196233. Epub 2009/02/07. eng.
- 765 61. Danielson NB, Kaifosh P, Zaremba JD, Lovett-Barron M, Tsai J, Denny CA, et al.  
766 Distinct contribution of adult-born hippocampal granule cells to context encoding. *Neuron*.  
767 2016;90(1):101-12.
- 768 62. Dieni CV, Panichi R, Aimone JB, Kuo CT, Wadiche JI, Overstreet-Wadiche L. Low  
769 excitatory innervation balances high intrinsic excitability of immature dentate neurons. *Nature*  
770 *communications*. 2016;7:11313. PubMed PMID: 27095423. Pubmed Central PMCID:  
771 PMC4843000. Epub 2016/04/21. eng.
- 772 63. Marin-Burgin A, Mongiat LA, Pardi MB, Schinder AF. Unique processing during a  
773 period of high excitation/inhibition balance in adult-born neurons. *Science*. 2012 Mar  
774 9;335(6073):1238-42. PubMed PMID: 22282476. Pubmed Central PMCID: PMC3385415. Epub  
775 2012/01/28. eng.
- 776 64. de la Rocha J, Doiron B, Shea-Brown E, Josic K, Reyes A. Correlation between neural  
777 spike trains increases with firing rate. *Nature*. 2007 Aug 16;448(7155):802-6. PubMed PMID:  
778 17700699. Epub 2007/08/19. eng.
- 779 65. Aronov D, Victor JD. Non-Euclidean properties of spike train metric spaces. *Physical*  
780 *Review E*. 2004 06/02/;69(6):061905.
- 781 66. Motulsky HJ, Ransnas LA. Fitting curves to data using nonlinear regression: a practical  
782 and nonmathematical review. *FASEB journal : official publication of the Federation of*  
783 *American Societies for Experimental Biology*. 1987 Nov;1(5):365-74. PubMed PMID: 3315805.  
784 Epub 1987/11/01. eng.



**Fig 1. Pattern separation assay in acute brain slices at the single cell level.**

**(A)** Five input sets out of eleven used. *Top*: rasters of the five spiketrains of each set. *Bottom*: correlation coefficient matrix for each input set, each square representing the correlation coefficient between two input spiketrains measured with a binning window of 10 ms (color scale at left). Traces are ordered by decreasing similarity (i.e. coefficient average, diagonal excluded) from  $R_{\text{input}} = 0.95$  (far left) to  $R_{\text{input}}=0.11$  (far right).

**(B)** Histology of the DG in a horizontal slice (Cresyl violet/Nissl staining; scale bar: 250 $\mu\text{m}$ ), overlaid with a schematic of the experimental setup: a theta pipette in the ML (input) is used to focally stimulate the PP while a responding GC (output) is recorded via whole-cell patch-clamp. (GCL: granule cell layer, H: hilus, ML: molecular layer, FS: fast-spiking interneuron. Solid lines represent dendrites and dashed lines axons)

**(C)** Current-clamp recordings of the membrane potential of two different GCs in response to different input sets (*Top*:  $R_{\text{input}} = 1$ ; *Bottom*:  $R_{\text{input}} = 0.76$ ). Each set of five input traces is repeated ten times (only 3 repetitions are shown, with spikes truncated at 0 mV). In the bottom graph, input trains and their respective children output spiketrains have matching colors.

**Fig 2. Input spiketrains are decorrelated at the level of individual granule cells.**

**(A)** Example of a recording set (input set + output set): the raster plot shows one set of input spiketrains and the children output spiketrains recorded from one GC, organized so that output subsets (i.e., the ten children coming from one parent input spiketrain) are together and of the same color.

**(B)** Corresponding 55x55 correlation coefficient matrix using a binning window ( $\tau_w$ ) of 10 ms. Each small square represents the correlation coefficient between two spiketrains.  $R_{\text{output}}$  is defined as the mean of correlations between individual output spiketrains driven by different input spiketrains, as outlined by the bold blue border, which excludes comparisons between outputs generated from the same parent input.

**(C)** For each of the 102 recording sets (blue dots),  $R_{\text{output}}$  was lower than  $R_{\text{input}}$ . Black dots and error bars represent means and SEM (as in D and E).

**(D)** *Left:* effective decorrelation averaged over all recording sets as a function of  $R_{\text{input}}$ . Although there is a significant decorrelation for all tested input sets (one-sample T-tests: the blue shade indicates the 95% confidence interval that average decorrelation is significantly above 0), they are effectively decorrelated to different magnitudes (one-way ANOVA,  $p < 0.0001$ ). *Right:* post-hoc Tukey-Kramer tests show that the decorrelation is significantly different (higher) for highly similar input spiketrains than for already dissimilar inputs.

**(E)** When the effective decorrelation is normalized to the correlation of the input set, there is no significant difference between input sets (ANOVA,  $p = 0.18$ ).

In all graphs,  $\tau_w = 10$  ms.

**Fig 3. Orthogonalization of input spiketrains is a strong component of temporal pattern separation by single granule cells.**

(A-C) Three hypothetical cases of pairs of spiketrains and their associated correlation coefficients (R), normalized dot products (NDP) and scaling factors (SF), showing that the three metrics are not equivalent.

(A) Synthetic spiketrains (X and Y pairs) divided into six bins, with the corresponding number of spikes per bin.

(B) R between each pair of X and Y describes the linear regression between the number of spikes in the bins of X versus the corresponding bins in Y (jitter was added to make all points visible).

(C) Geometric view of vectors X and Y, where each bin is a dimension of a 6-dimensional space, and the number of spikes in a bin is the coordinate along this dimension. NDP measures how close to orthogonal two spiketrains are and SF measures how different their binwise firing rates are.

(D) Vector representation of experimental data from one recording set, showing the average similarity between a set of input spiketrains (dashed line and green angle,  $R_{\text{input}} = 0.76$ ) and the average similarity between the fifty corresponding output spiketrains (solid line, purple angle, over the same subsets as enclosed in the blue border in **Fig 2B**). The angles are derived from the NDP whereas the lengths of each vector express differences in binwise firing rates (SF). Here, outputs are more orthogonal (closer to  $90^\circ$ ) than their inputs with little difference in scaling.

(E-F)  $\text{NDP}_{\text{output}}$  or  $\text{SF}_{\text{output}}$  as a function of  $\text{NDP}_{\text{input}}$  or  $\text{SF}_{\text{input}}$ . Mean and SEM in black.

(E) All data points (102 recording sets) are below the dashed identity line indicating that outputs are closer to orthogonality ( $\text{NDP} = 0$ ) than their respective inputs. The average orthogonalization ( $\text{NDP}_{\text{input}} - \text{NDP}_{\text{output}}$ ) is significant for all input sets (one-sample T-tests,  $p < 0.05$ ).

(F) Most points fall slightly below the dashed identity line, suggesting that pattern separation by scaling of the binwise firing rate is present but weak at  $\tau_w = 10\text{ms}$ . The average scaling ( $SF_{\text{input}} - SF_{\text{output}}$ ) is significant for all input sets except the three most dissimilar ( $SF_{\text{input}} = 0.88, 0.89, 0.90$ ) (one-sample T-tests,  $p < 0.05$ ).



**Fig 4. Single granule cells perform pattern separation on millisecond to second timescales using different codes.**

**(A) Top:** Average  $R_{\text{output}}$  as a function of  $R_{\text{input}}$ , measured with different time windows  $\tau_w$ . Solid curves are fitted parabolae. Each color corresponds to a different  $\tau_w$  ranging from 5 ms to 100 ms. **Bottom:** Effect of  $\tau_w$  on the effective decorrelation, interpolated from the parabolic regressions.

**(B)** Same as A but using NDP and linear regressions. **Bottom:** Note that the timescale axis is extended to 2000 ms, with the inset showing an expansion over the shorter timescales).

**(C)** Same as B using SF.

**(B-C)** Note that as  $\tau_w$  increases, pattern separation through orthogonalization becomes weaker but stronger through scaling.

**(D)** Similarity between spiketrains is here assessed with the binless SPIKE metric, directly using spike times. **Left:** example of two input spiketrains associated with two output spiketrains from a GC recording set, and the corresponding distances  $D(t)$  between spiketrains.  $D(t)$  can then be integrated over time to give a single value  $D$ . **Middle:** example of 55x55 matrix of SPIKE similarity ( $1-D$ ) between all spiketrains of an example recording set. 0 means that spikes of two trains never happened close in time, and 1 that they were perfectly synchronous. The output SPIKE similarity ( $\text{SPIKE}_{\text{output}}$ ) is defined the same way as for  $R$ , NDP or SF (average of the values inside the blue border). **Right:**  $\text{SPIKE}_{\text{output}}$  of all GC recordings as a function of their input similarity ( $\text{SPIKE}_{\text{input}}$ ), fitted with a parabola (red line). Most data points are below the dashed identity line indicating that output spiketrains are less similar than inputs. The average  $\text{SPIKE}_{\text{input}} - \text{SPIKE}_{\text{output}}$  is significantly above 0 for all input sets except the two most dissimilar ( $\text{SPIKE}_{\text{input}} = 0.74, 0.78$ ) (one-sample T-tests,  $p < 0.05$ ).

**Fig 5. Input spiketrains are efficiently separated upon their first presentations.**

**(A)** Two of five inputs are shown with corresponding output spiketrains. The first output sweep is marked with a pink bar (right) and last sweep is marked with a blue bar.

**(B)**  $R_{\text{output}}$ , computed from the first sweep of five output trains only (pink), as a function of  $R_{\text{input}}$ , fitted with a parabola. All data points are below the identity line indicating that outputs are effectively decorrelated compared to their inputs even when input patterns have only been presented once each. The average decorrelation ( $R_{\text{input}} - R_{\text{output}}$ ) is significant for all input sets (one-sample T-tests,  $p < 0.01$ ) except for  $R_{\text{input}} = 0.11$  ( $p = 0.1$ ).

**(C)** *Left:* Average output correlations between spiketrains of the first sweep (pink) and the last sweep (blue). There is no significant difference (F-test comparing the two distributions using parabolic regressions,  $p = 0.47$ . Error bars are SEM). *Right:* When taking into account that the two distributions are paired, we detect that a few output correlations are significantly lower for the last sweep than for the first one (one-sample T-test on the difference between  $R_{\text{output}}$  of the first and last sweep of each recording set, asterisks signify  $p < 0.05$ ). This is evidence, though weak, that repetition of input spiketrains might improve pattern separation for highly similar inputs.

**Fig 6. Pattern separation in single GCs is not explained by simple neural noise.**

**(A)** The variability of output spiketrains in response to the same input train sets the upper bound for  $R_{\text{output}}$ . *Left*: Correlations between pairs of output spiketrains associated with different input trains (enclosed by red,  $R_{\text{output}}$ ) and pairs of different output spiketrains associated with the same input train (enclosed by green,  $R_w$ : spiketrain reliability, the reproducibility of the output given the same input). *Right*: Empirical probability distribution of  $R_w$  for all recordings (dark green line is the mean:  $\langle R_w \rangle = 0.3$ ), overlaid on the distribution of  $R_{\text{output}}$  as a function of  $R_{\text{input}}$  (102 recording sets) fitted with a parabola. Note that means  $\langle R_w \rangle$  and  $\langle R_{\text{output}} \rangle$  for  $R_{\text{input}} = 1$  are close because they both assess the reproducibility of the output when the input is the same.

**(B)** Characterization of neural noise. *Top*: example of input and output spiketrains illustrating variable delay of the response spike after an input spike ( $d_1 < d_2$ ) or failure to spike after an input spike (red cross). *Bottom*: Example from one GC recording. The spike-wise noise in output spiketrains is characterized by the average spike delay, the standard deviation of this delay (jitter) and the probability of spiking after an input spike (spiking reliability of the cell, SR).

**(C-D)** Effect of random shuffling on  $R_{\text{output}}$  and  $R_w$ .

**(C)** Patterns are *less* separated for GC than for random shuffling (F-test using parabolic regressions:  $p < 0.0001$ ). **(D)** GC output is *more* reliable than for random shuffling (unpaired T-test,  $p < 0.0001$ ; mean  $\langle R_w \rangle_{\text{shuffle}} = 0.19$ ).

**(E)** Paired statistical tests show that shuffling leads to smaller  $R_{\text{output}}$  and  $R_w$  than original recordings. *Top*: paired T-test on all recording sets,  $p < 0.0001$ . *Bottom*: one-sample T-test on difference between shuffled and original data  $R_{\text{output}}$  performed on each  $R_{\text{input}}$  group. Black symbols correspond to the means, bars to SEM. The purple shade indicates the 95% confidence interval. Asterisks signify  $p < 0.001$ .

**Fig 7. Unreliability in spiketrain transmission is a major but not unique source of temporal pattern separation.**

(A) Spiketrain reliability ( $R_w$ ) is an excellent predictor of normalized decorrelation (defined in **Figure 2E**). Green: 102 recording sets from GC recording sets; Red: 20 recording sets from fast-spiking interneurons (FS). Notice that, despite the strong anti-correlation, the affine model predicts that even a perfect reliability ( $R_w = 1$ ) could still allow 10% of decorrelation. See **Table 3** for linear regressions on GCs or FS alone.

(B) The ten children output spiket trains of each of the five inputs can be averaged to give the five output peristimulus histograms (PSTH) corresponding to the five input trains. The 10 ms binned PSTHs of the output rasters in **Fig 2A** are shown.

(C) Correlation coefficients between all pairs of the five output PSTHs. The mean correlation (PSTH  $R_{\text{output}}$ ) is the average of coefficients inside the red border, and excludes self-comparisons.

(D) *Left*: PSTH  $R_{\text{output}}$  as a function of  $R_{\text{input}}$  (102 recording sets, in red), fitted with a parabola (black). All points are below the identity line indicating decorrelation of outputs compared to inputs. *Right*: Average effective decorrelation ( $R_{\text{input}} - \text{PSTH } R_{\text{output}}$ ) as a function of  $R_{\text{input}}$  (bars are SEM) reveals a significant decorrelation for all input sets except for the most dissimilar (one-sample T-tests; shaded area is the 95% confidence interval for significant decorrelation).

(E) Averaged PSTH  $R_{\text{output}}$  as a function of  $R_{\text{input}}$ , for different binning windows  $\tau_w$ .

**Fig 8. Fast-spiking interneurons of the DG exhibit lower levels of pattern separation than GCs.**

(A) Picture of a recorded FS filled with biocytin (black). In the case of simultaneous recordings, the recorded GCs were close to the FS, as depicted by the schematic in green.

(B-C) Example of a simultaneous whole-cell recording of a GC and a neighboring FS.

(B) Simultaneous membrane potential recordings (baseline around -60mV) of a FS and a GC to the same set of current steps (-25pA, 100pA, 500pA and 1000pA).

(C) Simultaneous current-clamp recordings of the same FS and GC as in A in response to the five input traces of an input set with  $R_{input} = 0.65$  (first sweep of five output trains). Simultaneous input and output trains have the same color.

(D)  $R_{output}$  versus  $R_{input}$  at  $\tau_w = 10$ ms. Data points correspond to recording sets: 20 for FS (red), and 61 for GC (green, with a darker shade open circle when simultaneously recorded with a FS). All GC recordings done at the same input correlations as FS recordings were used for an unpaired comparison:  $R_{output}$  distribution for FS is significantly higher in FS than in GC (F-test using linear regressions:  $p < 0.0001$  (asterisk); unbalanced two-way ANOVA, stimulation groups:  $p = 0.0015$ , cell-types:  $p < 0.0001$ , interaction:  $p = 0.72$ .) Post-hoc Tukey-Kramer tests: significant difference for stimulation groups with measured correlation  $R_{input} = 0.88, 0.84$  and  $0.74$  ( $p < 0.01$ ).

(E) Spiketrain reliability  $R_w$ . Same color code and recording sets as in D. Unpaired T-test:  $p < 0.0001$  (asterisk).

(D-E) Note that when comparing only the simultaneous GC and FS recordings, we found a similarly significant difference, both for  $R_{output}$  and  $R_w$ .

**Fig 9. Cell-to-cell comparisons show that granule cells have variable responses to identical inputs and perform pattern separation in different ways.**

**(A)** Spiketrain-wise comparison between recording sets.

**(A1)** The similarity between pairs of spiketrains coming from two different output sets but associated to the same input set and with the same sweep number is assessed with the Pearson's correlation coefficient ( $\tau_w = 10$  ms). The fifty resulting coefficients are then averaged to give  $R_{\text{cell-to-cell}}$ , a single number measuring the overall similarity of output spiketrains between two recording sets. All combinations of pairs of output sets from the same input set were compared.

**(A2)** Probability distribution of  $R_{\text{cell-to-cell}}$  (green line) across all GC recordings. The distribution of  $R_{\text{cell-to-cell}}$  (black circles) is not dependent on  $R_{\text{input}}$ .

**(A3)** Distribution of  $R_{\text{cell-to-cell}}$  for different cell-types. (GC to GC:  $n = 470$ , FS to FS:  $n = 30$ , FS to GC simultaneously recorded:  $n = 15$ ).

**(B)** Comparison of the pattern separation levels between recording sets.

**(B1)** Top: same as Fig. 2B but in grey scale. Colored squares enclose the coefficients comparing outputs in response to two different input trains which have a  $R_{\text{input}} \sim 0.76$  shown in (A1). Bottom: Average decorrelation of input spiketrains for each group of comparisons enclosed by the matching colored square above. Here, for each of these groups,  $R_{\text{output}}$  is the average of the coefficients in the square of the corresponding color and  $R_{\text{input}}$  is the correlation coefficient between the corresponding two parent input trains (not the average  $R$  over all input trains). For each recording set, a one-way ANOVA was performed to compare the 10 groups. For the GC shown, the ANOVA was significant, suggesting that levels of decorrelation depend on the identity of the input trains.

**(B2)** Percentage of recording sets with a significant ANOVA (crosses in black, axis on left). For all input sets except  $R_{\text{input}} = 1$  the proportion was high. The distribution of the largest difference between the mean of the ten decorrelation groups of a single recording set is also plotted (grey circles, axis on right).

**(B3)** To assess whether cells perform similar levels of pattern separation we computed  $R_{\text{cell-to-cell}}\{\text{decorr}\}$ , the Pearson's correlation coefficient between decorrelation groups (as in B1) from pairs of recording sets.

**(B4)** Distribution of  $R_{\text{cell-to-cell}}\{\text{decorr}\}$  (GCs only, mean and SEM in red). Like in **A**, all combinations of pairs from the same input set were compared (442 total comparisons).  $R_{\text{input}} = 1$  was excluded. This analysis shows that, in our experimental conditions, not all GC decorrelate input spiketrains the same way.

**S1 Fig. The correlation coefficient, normalized dot product and scaling factor between spiketrains do not have a simple relationship.**

(A-C) Two additional examples of hypothetical pairs (X and Y) of spiketrains divided into 6 bins, the number of spikes per bin constituting the numerical vector next to them (A right). The similarity between X and Y can be assessed by (B) the Pearson's correlation coefficient R describing the linear relationship between the number of spikes in corresponding bins or (C) by a vector analysis in a 6-dimensional space giving the angle between the vectors X and Y (computed from the normalized dot product, NDP) as well as the scaling factor (SF) between their norms. These examples provide the intuition that orthogonal vectors (NDP = 0) necessarily correspond to a negative correlation between the spiketrains but that anticorrelated spiketrains ( $R < 0$ ) are not necessarily orthogonal. Also, SF gives information about the firing rate per bin that R doesn't necessarily take into account (see second example in **Fig 3**).

(D) Relationships between these 3 similarity metrics (R, NDP and SF) computed between 1,000 randomly generated spiketrains with six bins like in (A) (All pairs combinations = 499,500 data points). For simplicity, each bin could have only 0, 1 or 2 spikes, which is why points in the SF graph are less distributed.

(E) Relationships between these three similarity metrics for 102 experimental GC recording sets. (124,950 data points)

(F) Relationship between these three similarity metrics averaged for each GC recording set (102 data points).

(E-F) Green lines correspond to a linear regression, the  $R^2$  and the p-value of which are indicated in each panel. Note that although R and NDP are well correlated in our experimental data



( $R^2 > 0.95$ ) (E-F left), there is not a linear relationship between R and NDP in theory (D left and see **Materials and methods**).

## **S2 Fig. Spike delay, jitter and reliability distributions for real data, simulations and shuffled data**

**(A)** Cross-occurrence method to measure spike delay, jitter and spiking reliability of a neuron during a given recording session. *Top:* Example histogram of output spikes occurring after input spikes, fitted (red curve) with a Gaussian distribution  $N(\mu, \sigma, \text{baseline})$ , where  $\mu$  is the mean delay and  $\sigma$  is the jitter of this delay. Lag 0 ms corresponds to the input spike time. In this example, output spikes are generated on average 16 ms after a stimulation impulse (delay) with a jitter ( $\sigma$ ) of 8.7 ms. *Bottom:* the baseline is subtracted and the histogram divided by the number of input spikes during the recording session. This gives the distribution of the probability of spiking after an input spike, the sum of probabilities defining the spiking reliability of the cell during the recording session. Here the neuron fires 39 % of the time after an input spike.

**(B-D)** Delay, jitter and spiking reliability (SR) distributions for (B) the original recordings, (C) the simulations and (D) the shuffled data set. Dashed horizontal red lines are means.

### **S3 Fig. Spike-wise neural noise characteristics are not good predictors of spiketrain decorrelation by single GCs.**

Plots of the normalized decorrelation, i.e.  $(R_{\text{input}} - R_{\text{output}}) / R_{\text{input}}$ , of each recording set ( $\tau_w = 10$  ms) : 102 for GC original and shuffled recordings (**A-B**), 20 for FS (**C**), as a function of spike-wise noise characteristics (spike delay, jitter and reliability). Solid green lines are the best linear fit, with  $R^2$  and p-values noted in each panel. These plots are examples to illustrate **Table 2**. Note that decorrelation is poorly explained (low  $R^2$ ) by either the spike delay or its jitter in all cell-types. In contrast, the spiking reliability (SR) is a good predictor of decorrelation in shuffled GC recordings (i.e. recordings entirely dominated by spike-wise noise) and even more so in FS recordings (for FS, SR was computed from nbFS data). This suggests that SR can be a potent mechanism for decorrelation, and that FS show different levels of decorrelation than GCs because they are more reliable. However, SR is only a mediocre predictor of decorrelation for GCs, thus confirming that temporal pattern separation in single GCs cannot be the result of simple neural noise.

#### **S4 Fig. Simulation of purely noisy outputs significantly decreases $R_{\text{output}}$ and spiketrain reliability**

Simulations of output spiketrains to the different input sets with random spiking following a Gaussian distribution defined by the mean spike delay, mean jitter and mean reliability of the original recordings.

**(A)** Pattern separation for different time windows  $\tau_w$  (dots: average  $R_{\text{output}}$  across all simulated "recordings" for a given input set, bars are SEM).

**(B)**  $R_{\text{output}}$  distribution at  $\tau_w = 10$  ms, for simulated data and original data. Distributions are fitted with parabolae and significantly different (F-test using parabolic regressions:  $p < 0.0001$ ).

**(C)**  $R_w$  distributions are significantly different (unpaired T-test,  $p < 0.0001$ ;  $\langle R_w \rangle_{\text{simul}} = 0.14$ ).

**(D)** Like in the original data (**Fig 2E**), the average normalized decorrelation  $((R_{\text{input}} - R_{\text{output}})/R_{\text{input}})$  seems invariant. Bars are SEM.

**(C-D)** Asterisks signify statistical significance

**S5 Fig. Differences in pattern separation between FS and GC are not solely due to FS bursting behavior or higher firing rate.**

(A) Probability of having 0, 1 or more output spikes between two input spikes assesses the bursting behavior in FS recordings.

(B) In contrast to GCs, for FS neurons there is a strong correlation between the firing rate of a recording set and the associated normalized decorrelation. See **Table 3** for linear regression goodness-of-fit and significance when considering GC only, or GC and FS combined.

(C) Example of bursts in a FS (*Bottom*) in response to input spikes (*Top*). To assess the effect of bursting on  $R_{\text{output}}$ , we truncated each recorded spiketrain from FS neurons to keep only the first output spike between two input spikes, thus removing any burst without altering the SR of the cell. The blue shaded areas highlight the spikes that were removed. The resulting truncated dataset was termed "nbFS" for "non-burst FS".

(D) The firing rate of nbFS neurons is significantly reduced compared to the firing rate of the original FS. (Kruskal-Wallis one-way ANOVA,  $p < 0.0001$ . FS vs nbFS (paired data): post-hoc Wilcoxon signed rank test with Bonferroni correction,  $p < 0.001$ ; nbFS vs GC (non-paired): post-hoc Mann-Whitney U-test with Dunn-Sidak correction,  $p = 0.02$ ; FS vs GC (non-paired): post-hoc Mann-Whitney U-test with Dunn-Sidak correction,  $p < 0.001$ ).

(E) Distributions of  $R_{\text{output}}$  ( $\tau_w = 10\text{ms}$ ). Data points correspond to individual recording sets of nbFS (purple) or GC (green). Both distributions are still significantly different, suggesting the bursting behavior of FS is not sufficient to explain the difference in pattern separation (Unbalanced two-way ANOVA. Stimulation groups:  $p = 0.002$ , cell-types:  $p < 0.0001$ , interaction:  $p = 0.84$ . Post-hoc Tukey-Kramer tests: nbFS and GC  $R_{\text{output}}$  are significantly different ( $p < 0.05$ ) for stimulation groups with measured correlation  $R_{\text{input}} = 0.88, 0.84, 0.74$ .)

**(F)** Distributions of  $R_w$  ( $\tau_w = 10$  ms) are still significantly different between GC and nbFS (unpaired T-test,  $p < 0.0001$ ). This suggests the bursting behavior of FS is not sufficient to explain the difference in spiketrain reliability  $R_w$ .

**(D-F)** Asterisks signify  $p < 0.001$ .

1 **S6 Fig. Fast-spiking interneurons and granule cells have different noise characteristics.**

2 **(A)** Cross-occurrence method (same as in **S2 Fig**) to measure spike delay, jitter and spiking  
3 reliability of nbFS neurons (to only consider the noise characteristics of the first spike, if there is  
4 a burst) *Top*: example of a histogram representing the number of output spikes occurring after  
5 input spikes. The histogram is fitted (red curve) with a Gaussian distribution  $N(\mu, \sigma, \text{baseline})$ ,  
6 where  $\mu$  is the mean delay and  $\sigma$  is the jitter of this delay. Lag 0 ms corresponds to the input  
7 spike time. In this example, output spikes are generated on average 7.8 ms after an input spike  
8 (delay) with a jitter of 4.2 ms. *Bottom*: the baseline is subtracted and the histogram divided by  
9 the number of input spikes during the recording session. This gives the distribution of the  
10 probability of spiking after an input spike of the cell during the recording session (SR). Here the  
11 neuron fires 59% of the time after an input spike.

12 **(B)** Delay, jitter, and SR distributions for the 20 nbFS recording sets. Dashed horizontal black  
13 lines represent means. To compare with **S2 Fig**.

14 **(C)** Comparison of the delay, jitter and SR between nbFS and GC recordings (Mann-Whitney U-  
15 tests,  $p < 0.0001$ ). FS first spike responses to a stimulation impulse is faster, has less jitter, and is  
16 more reliable than in GCs.

17

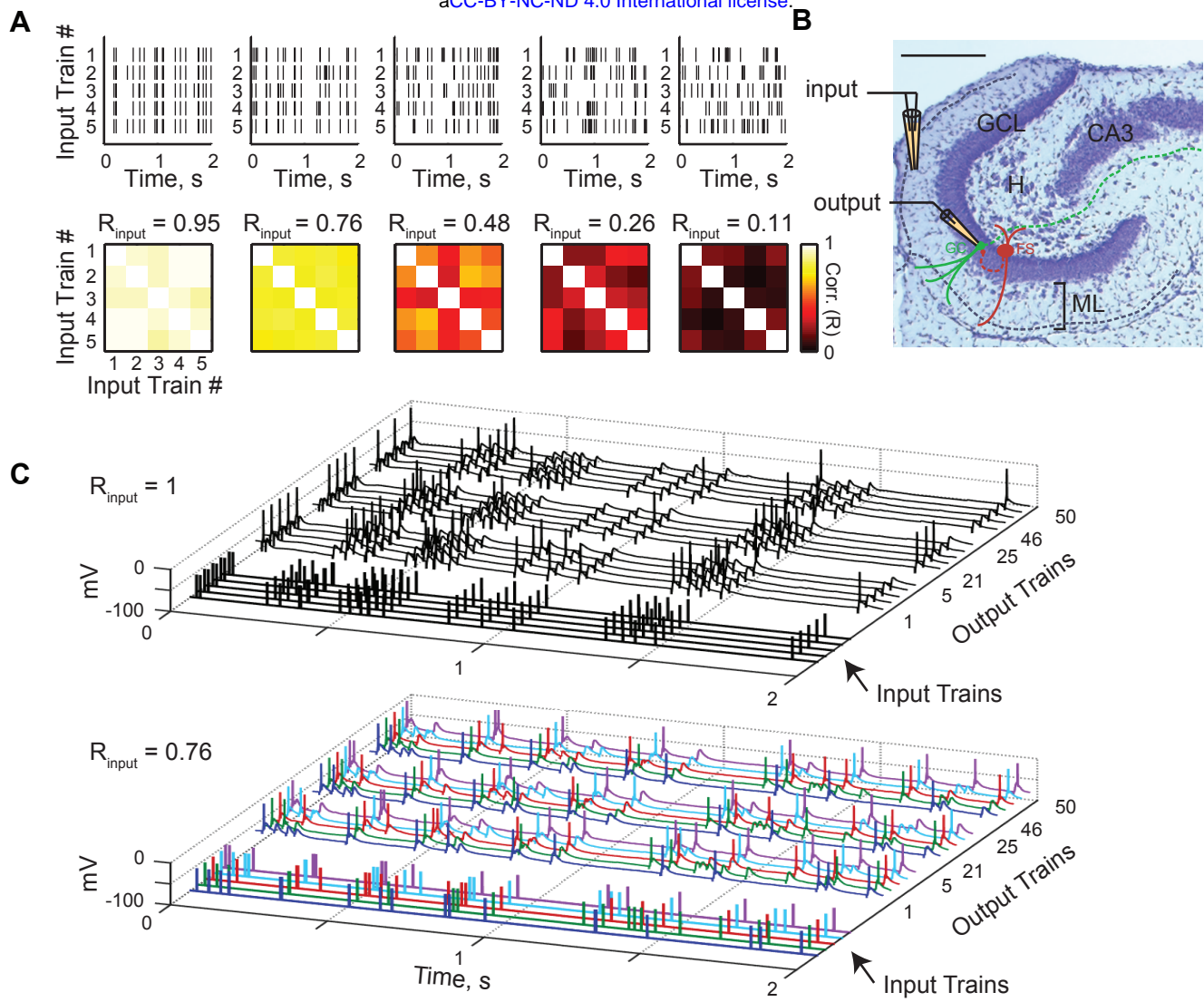


Figure 1



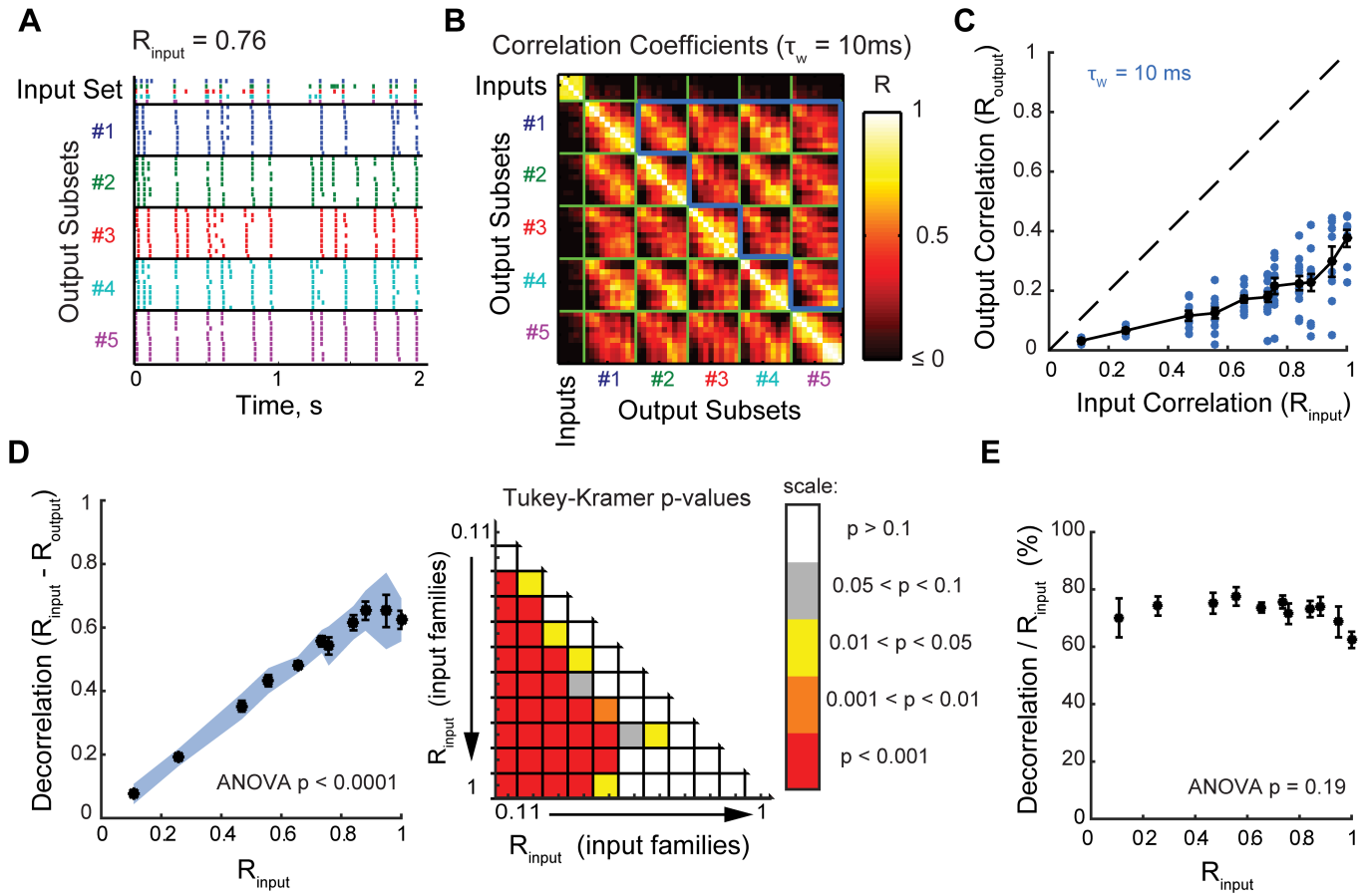


Figure 2

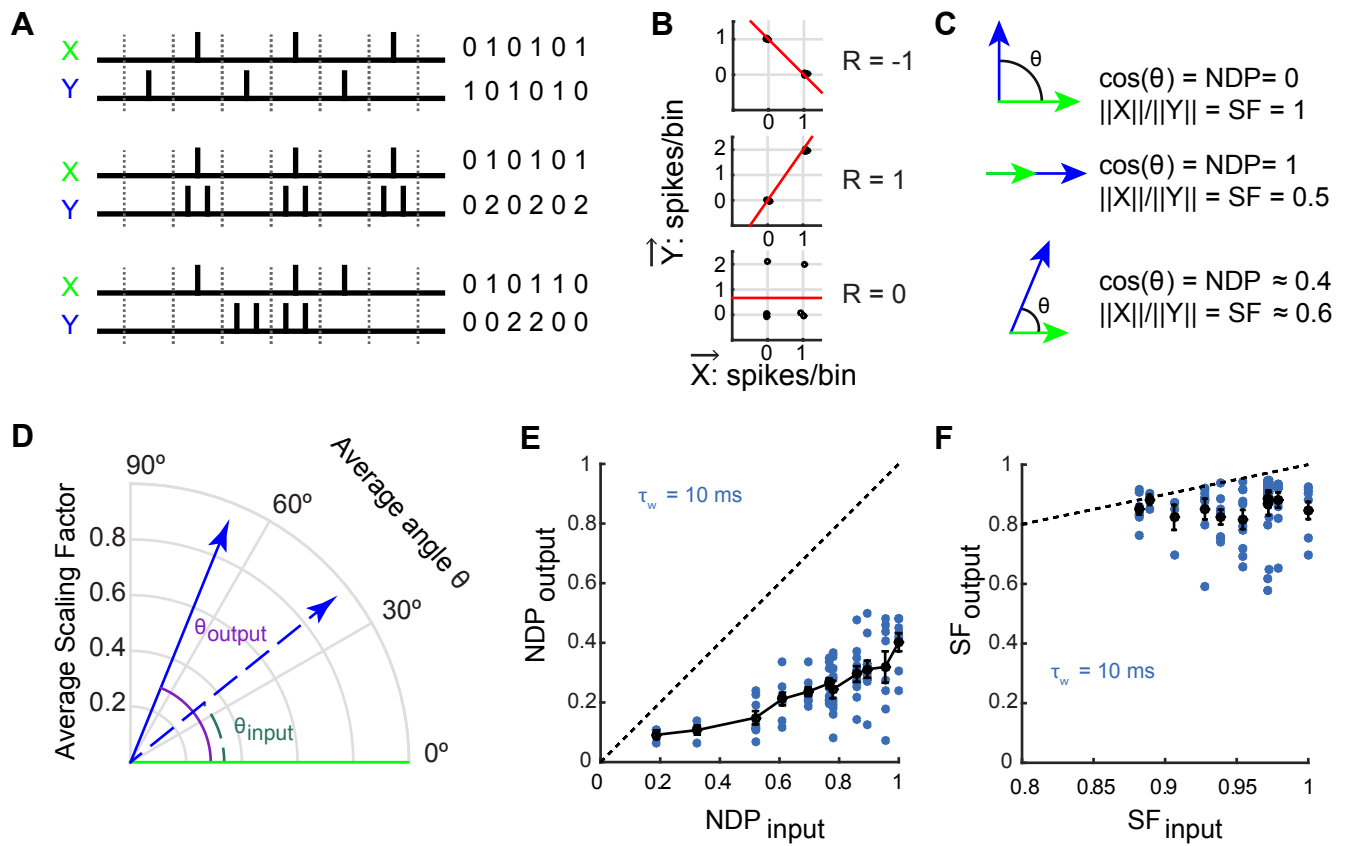


Figure 3

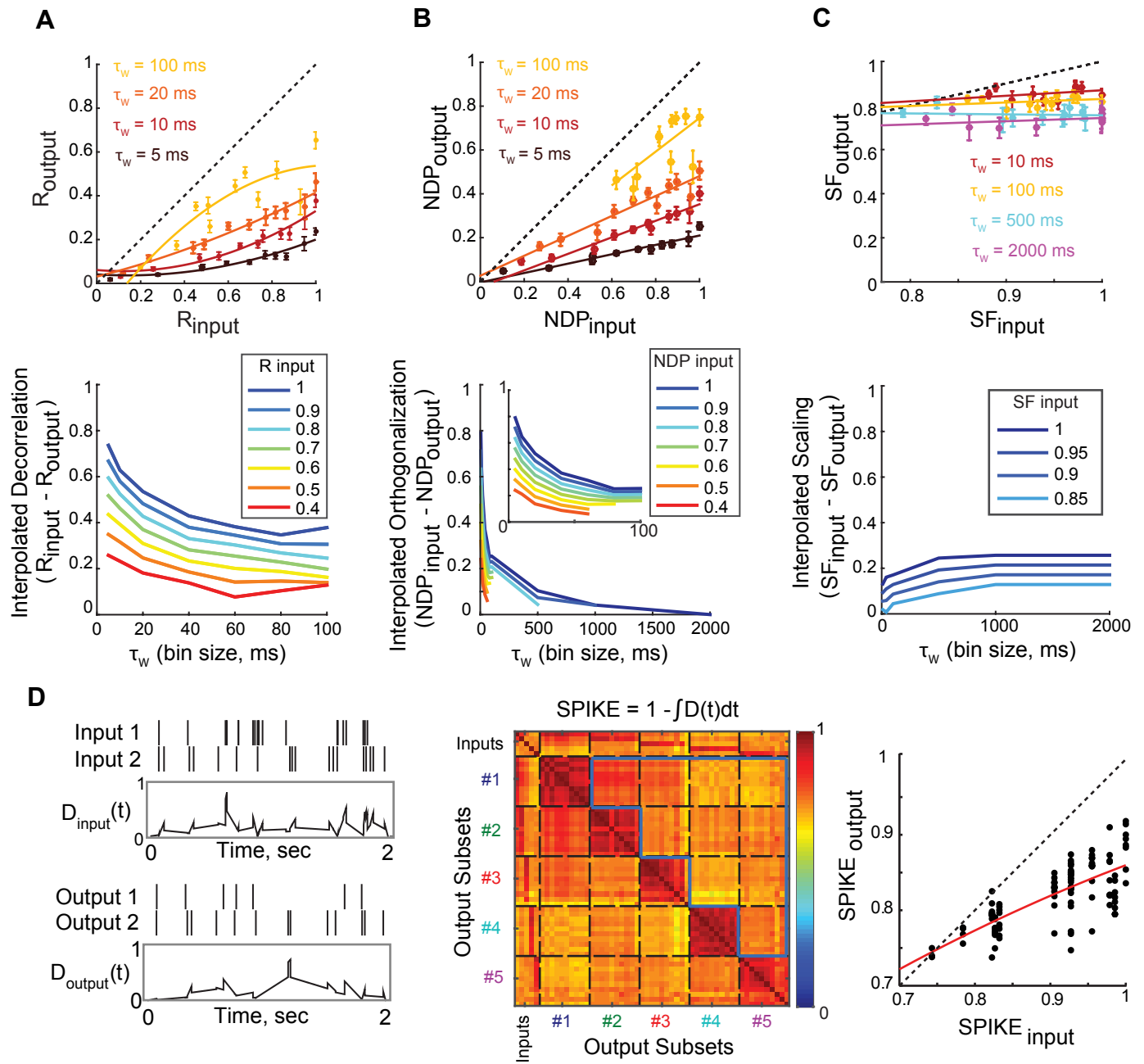


Figure 4

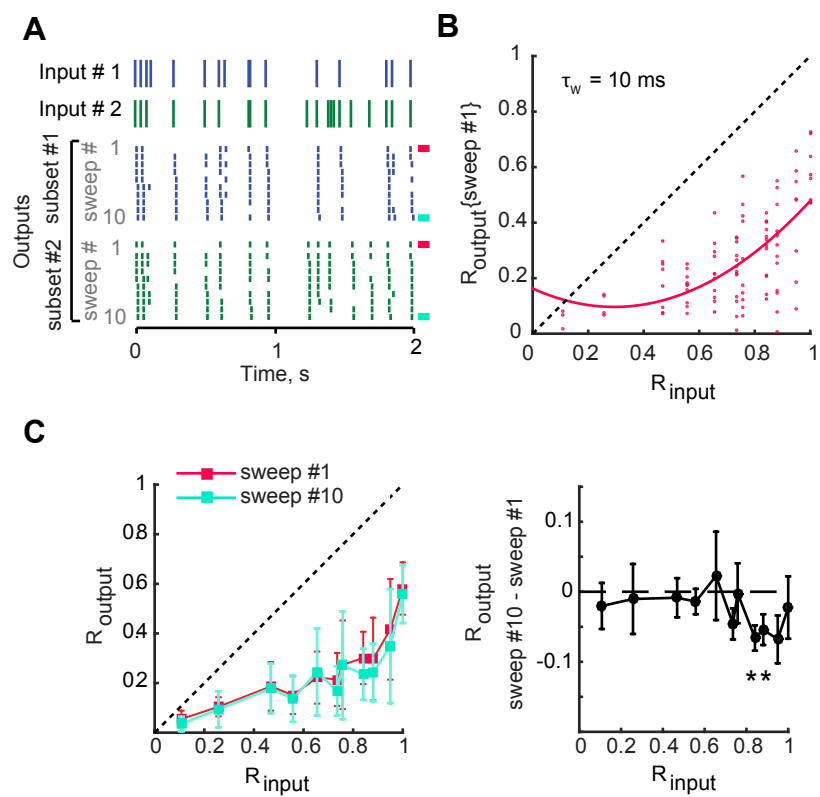


Figure 5

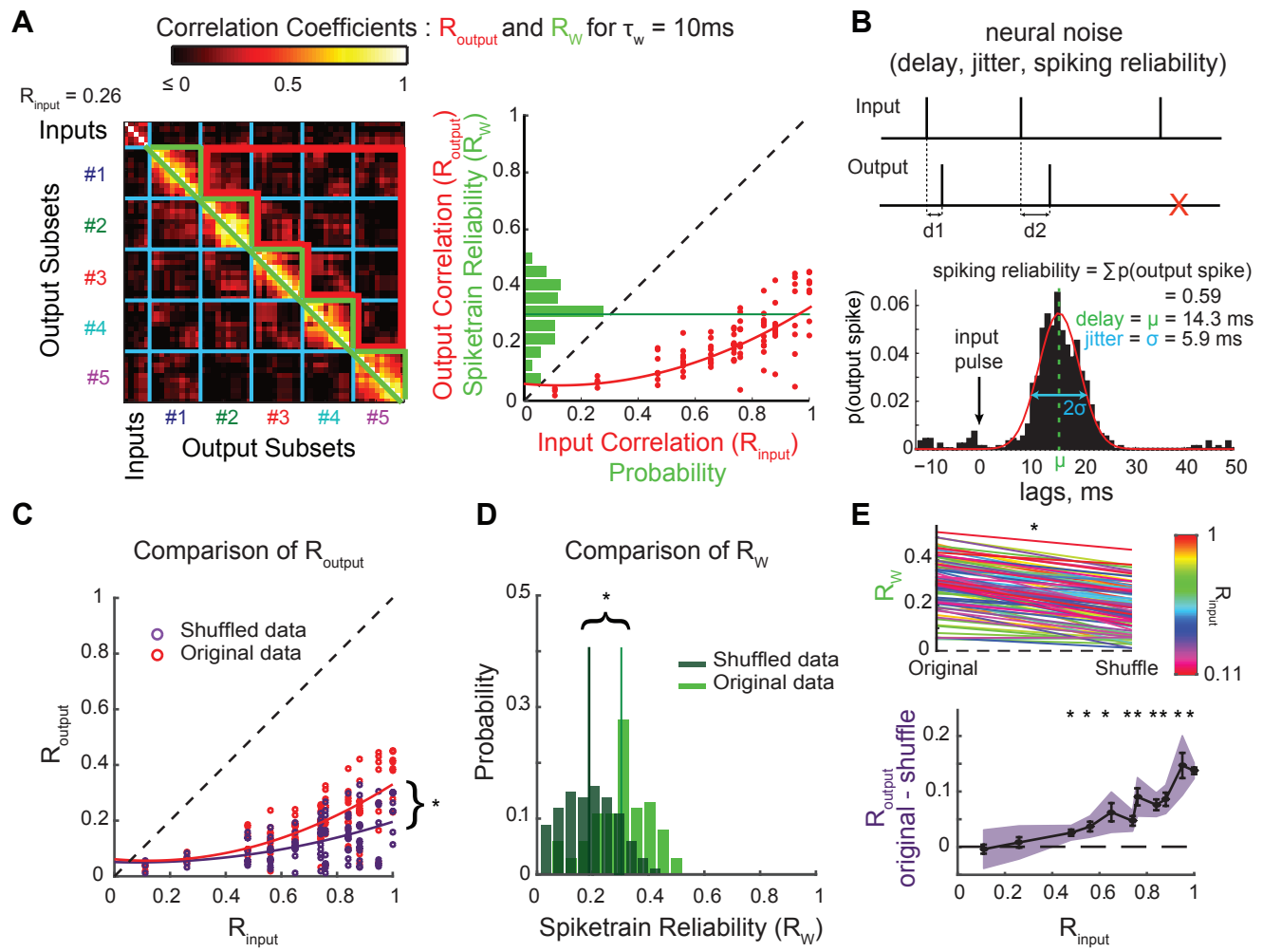


Figure 6

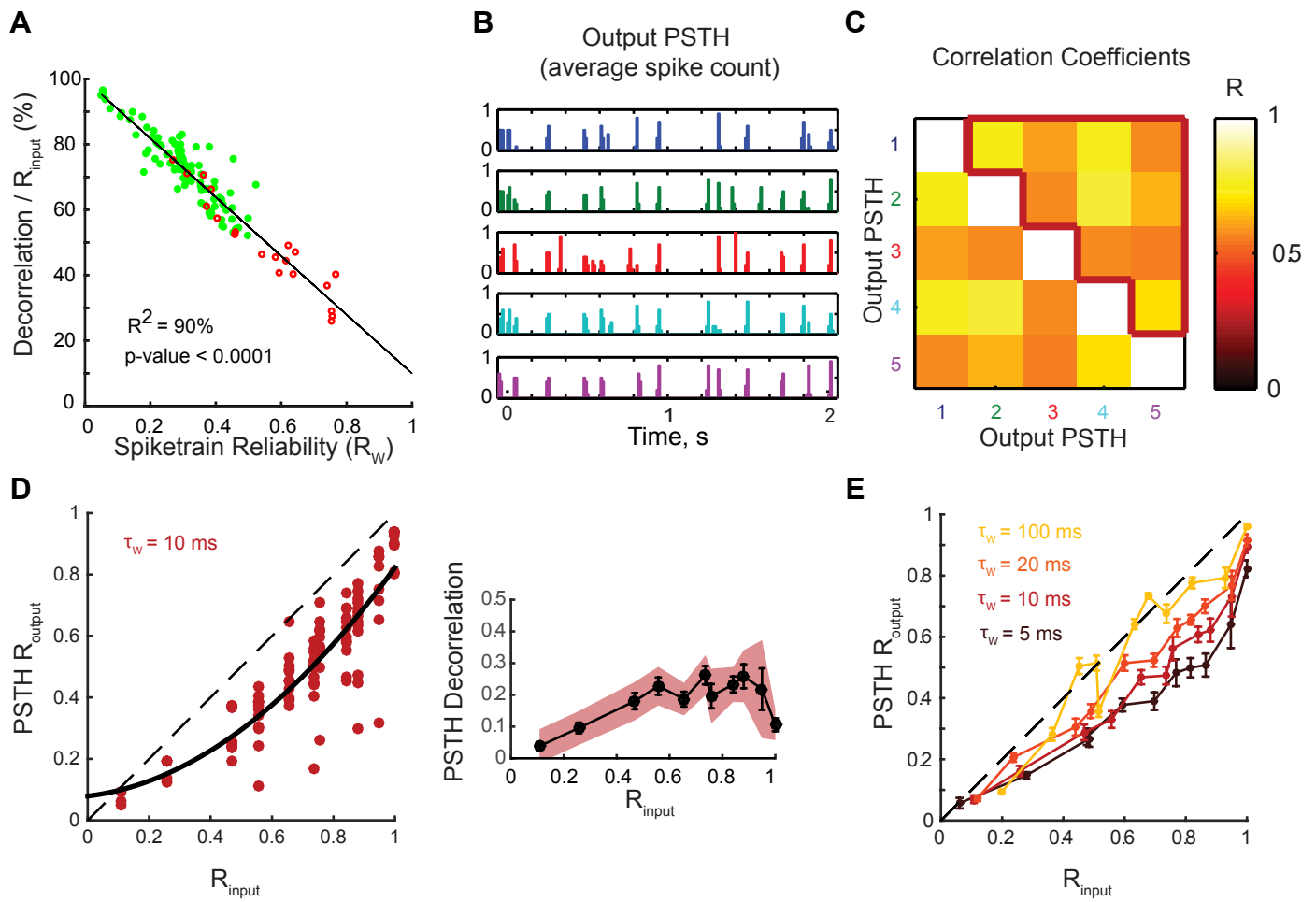


Figure 7

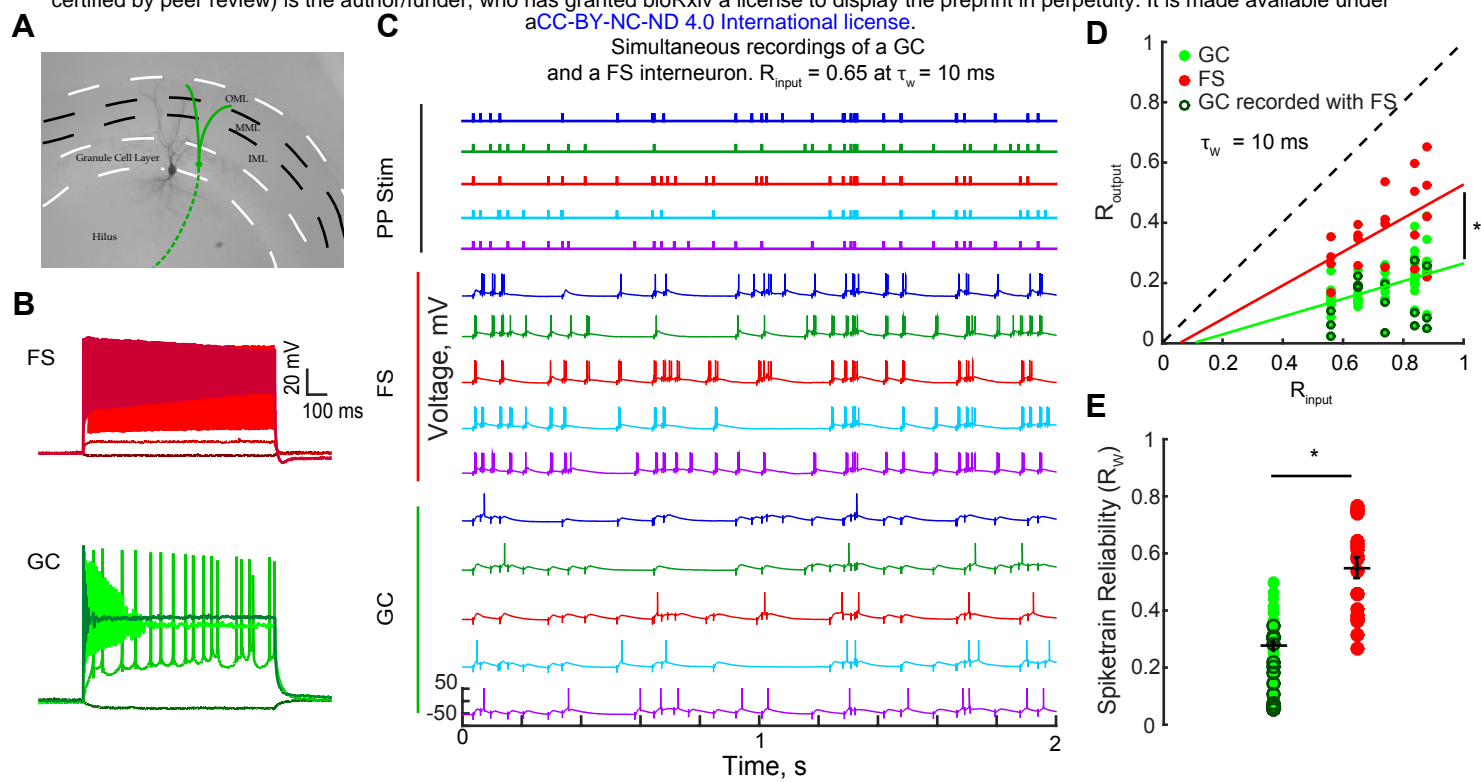


Figure 8

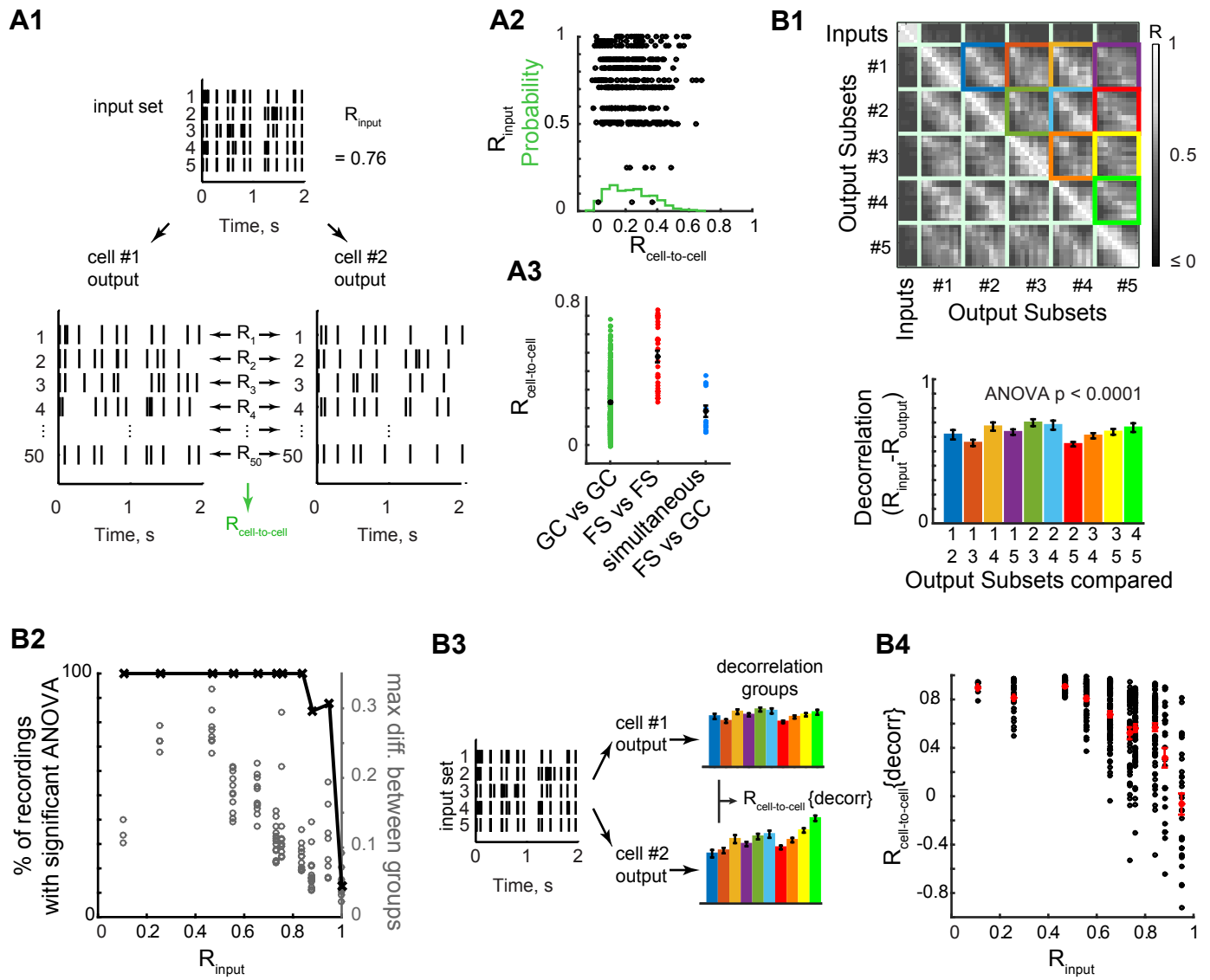
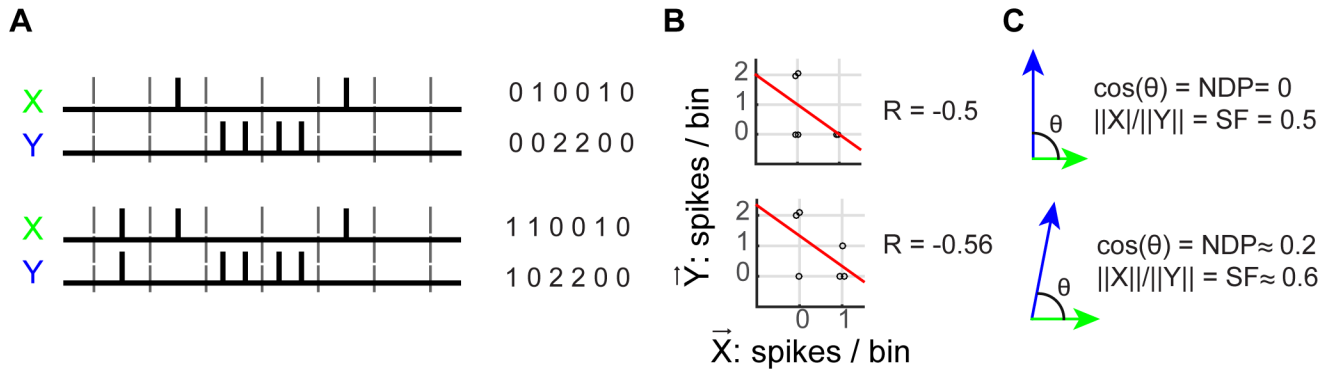
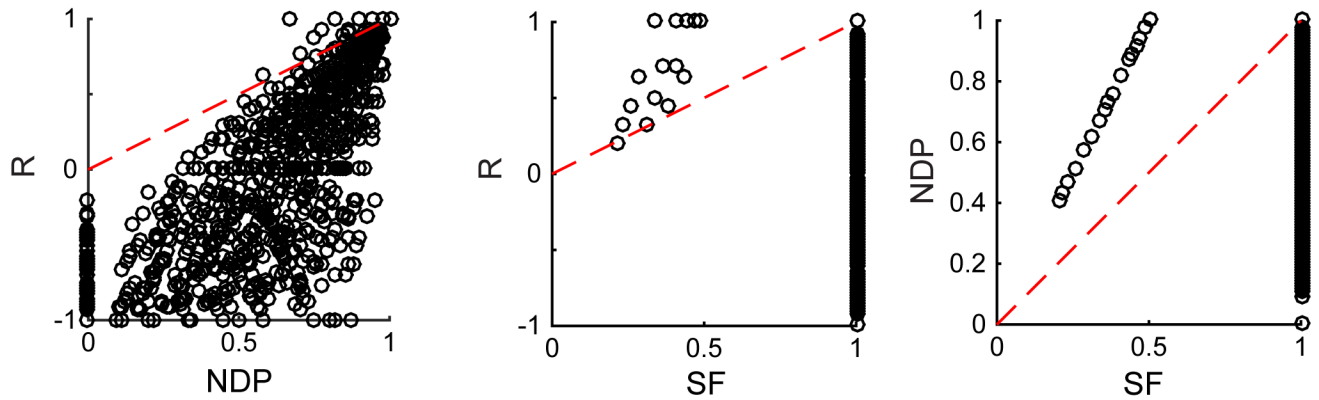


Figure 9

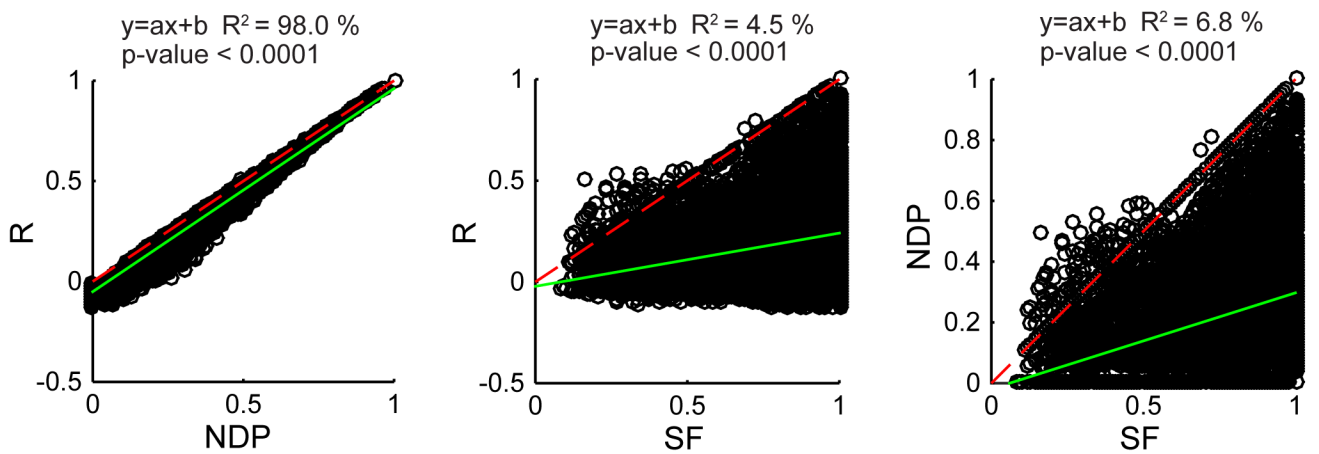




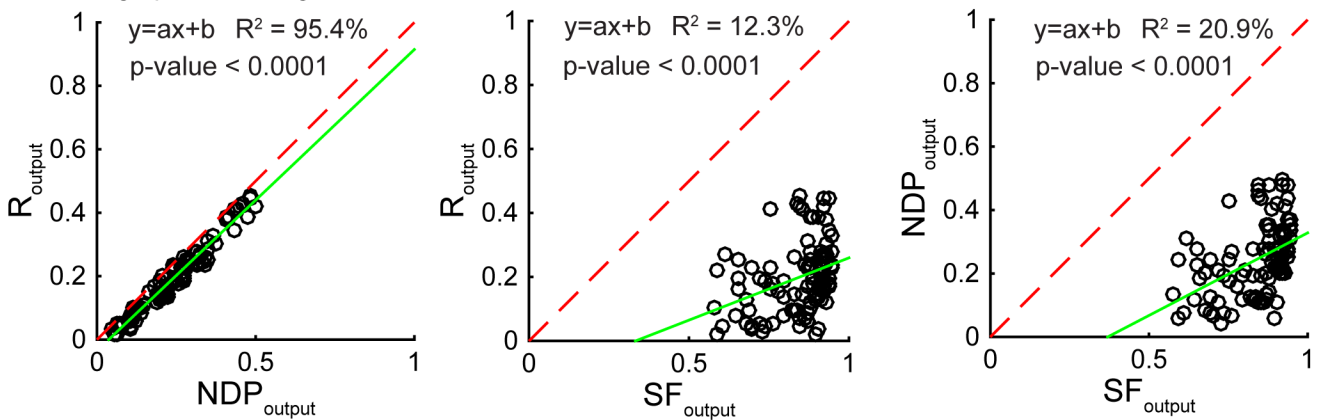
**D** Pairs of random synthetic spiketrains

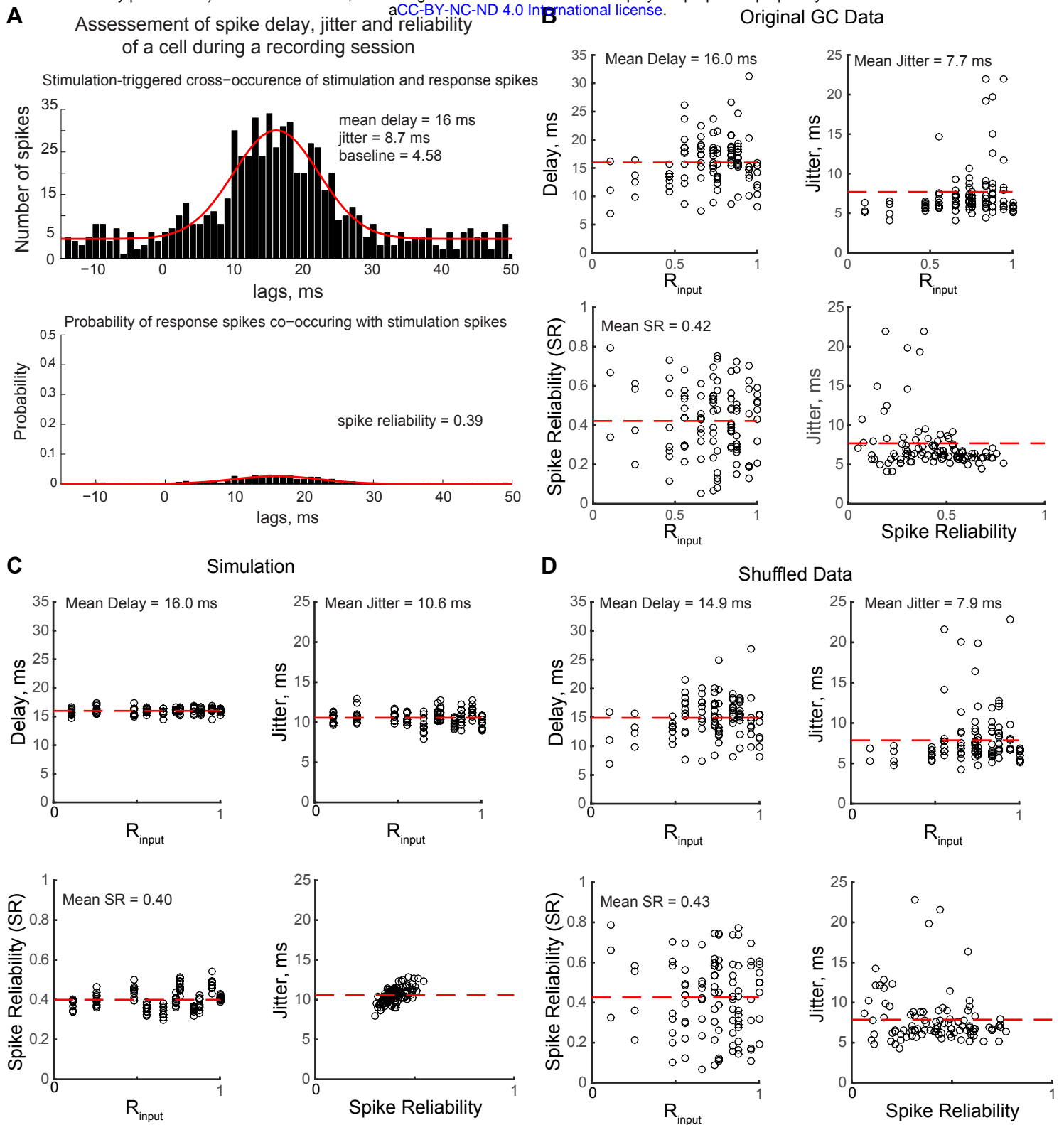


**E** Pairs of spiketrains from GC recordings

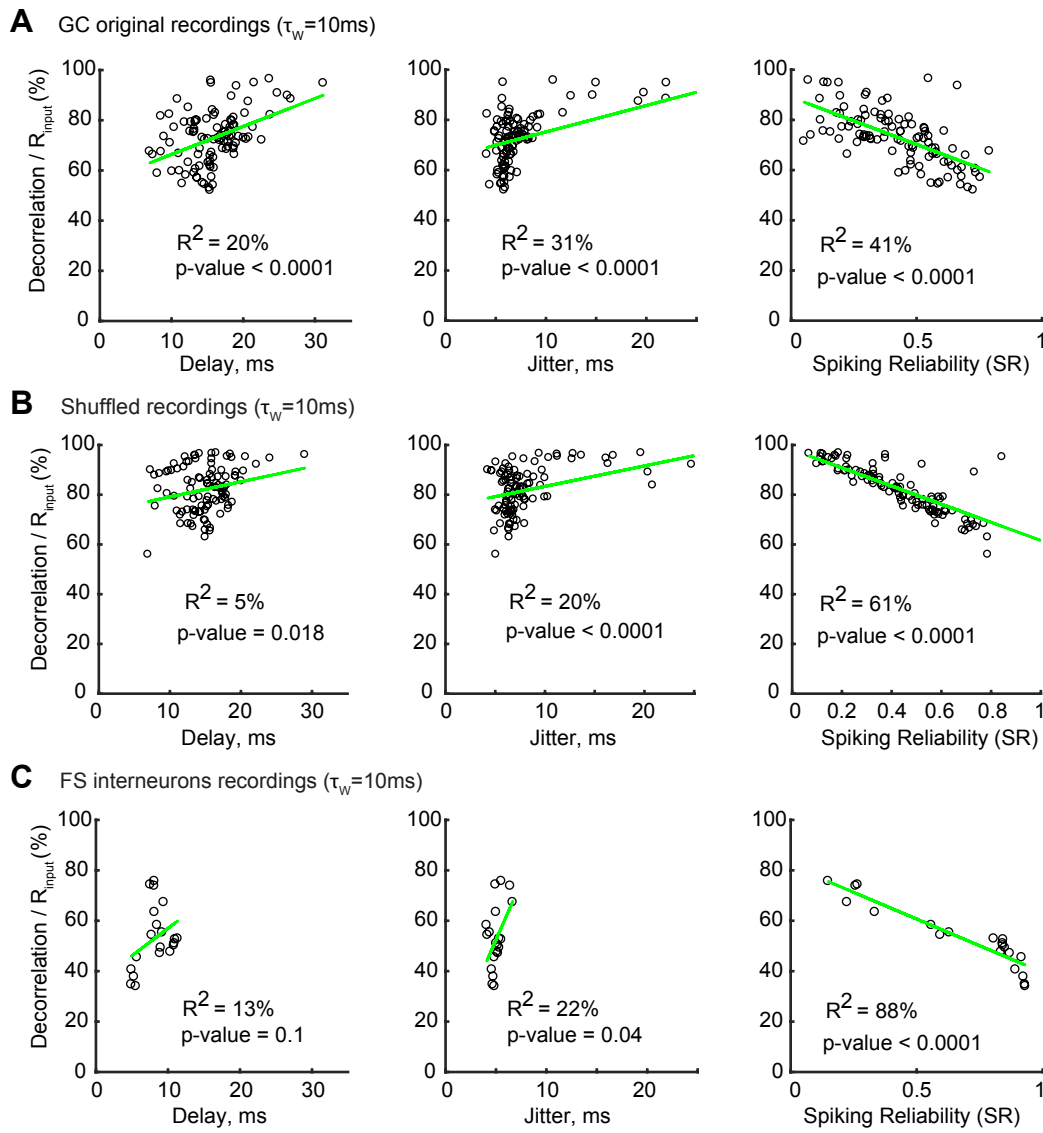


**F** Average per recording sets

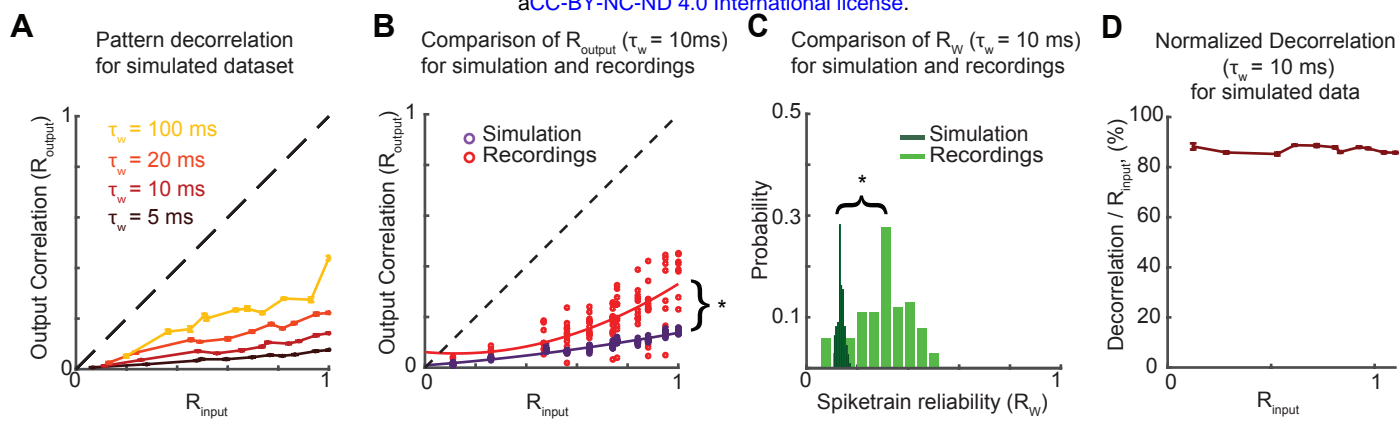




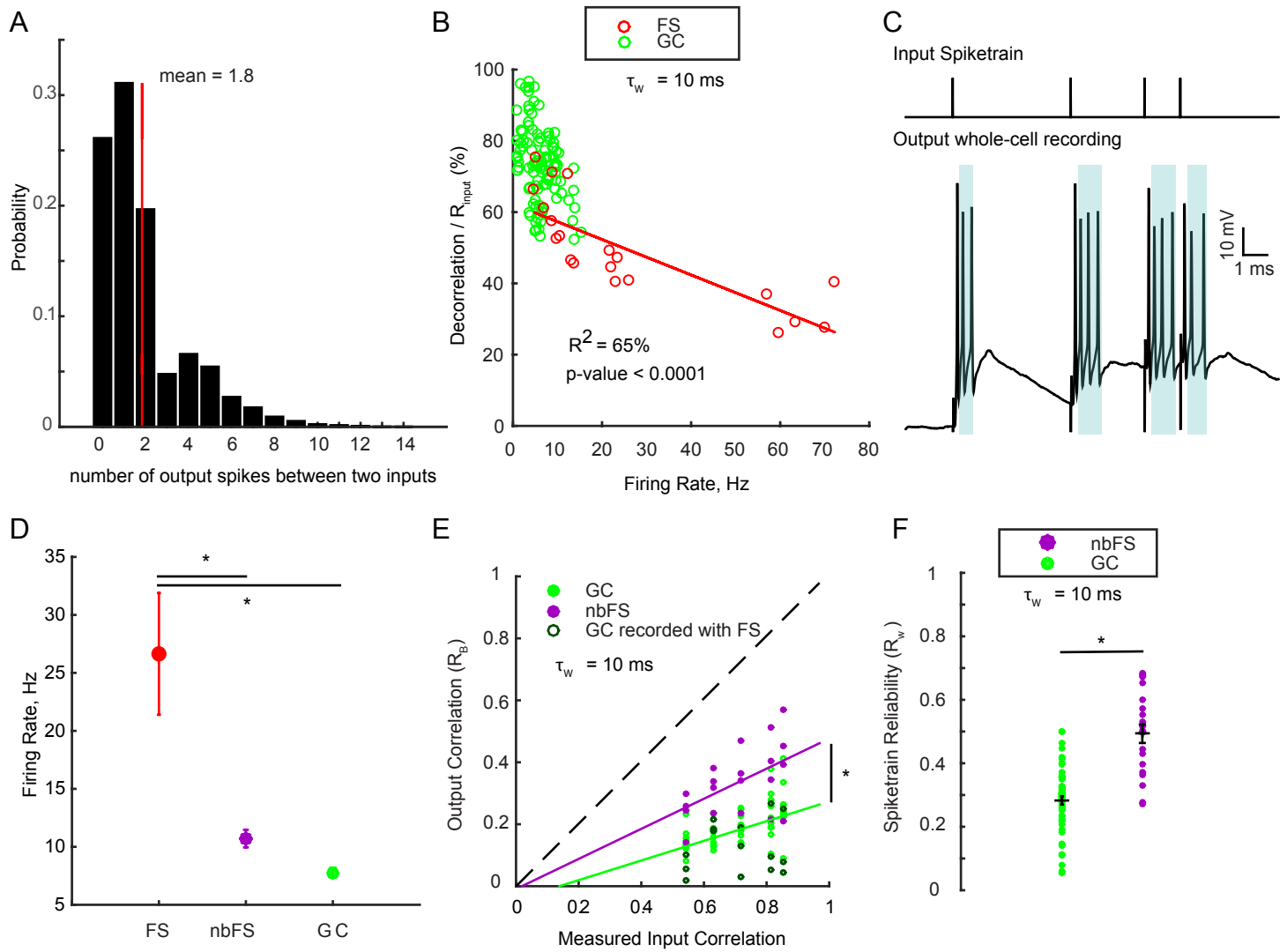
S2 Fig



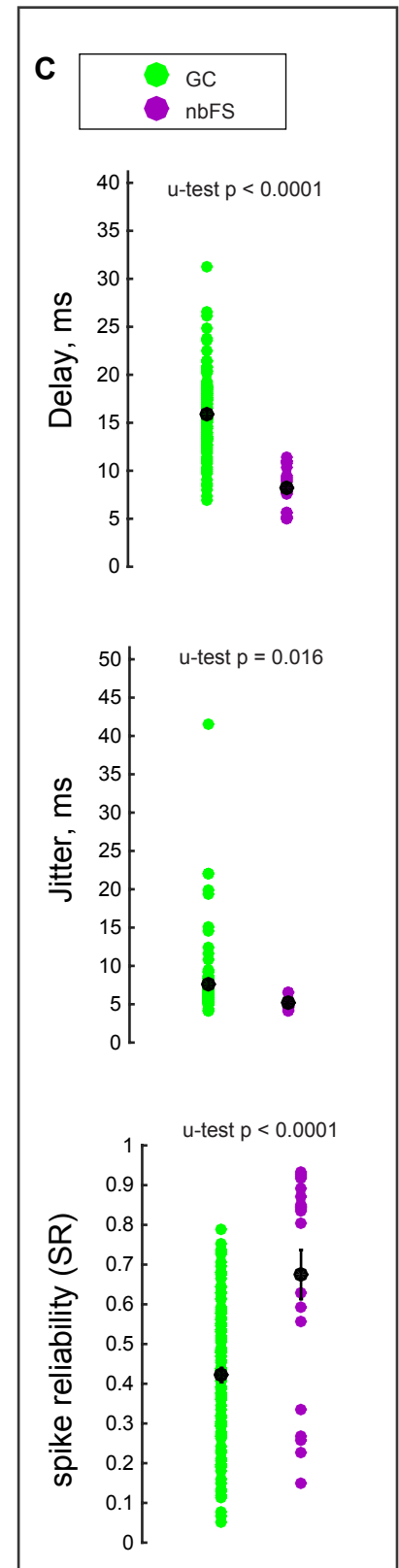
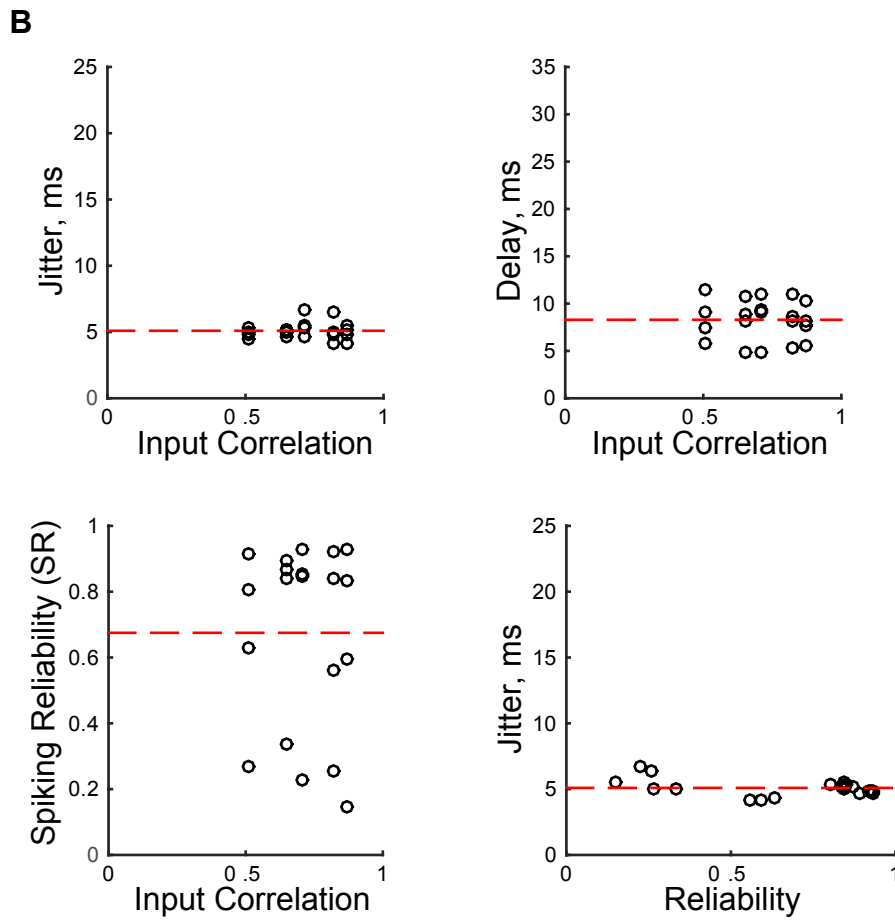
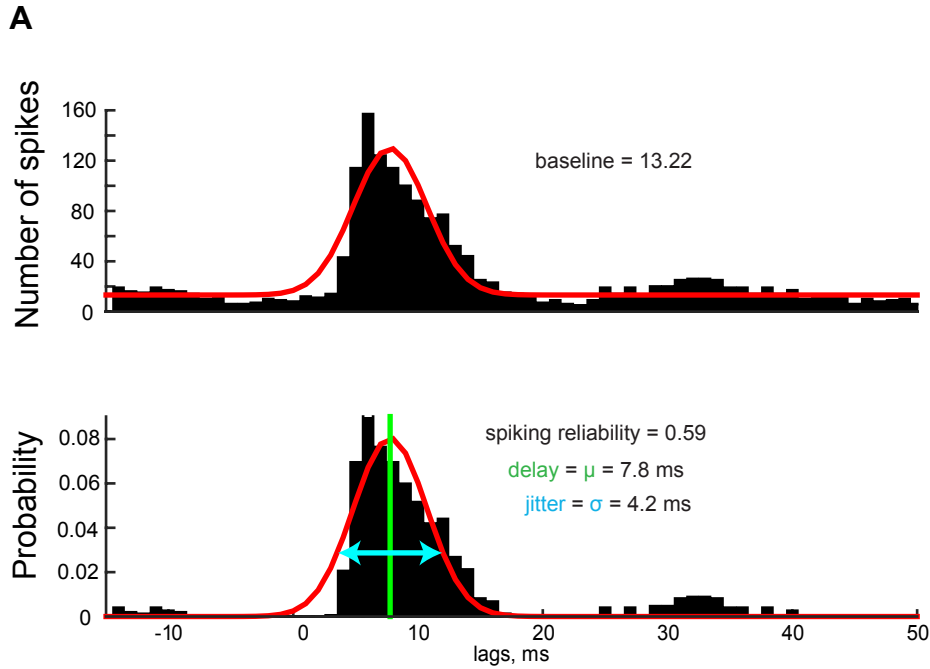
S3 Fig



S4 Fig



S5 Fig



S6 Fig

**Table 1-3. Linear regressions goodness-of-fit, p-value and slope.** The predictor variables (x-axis) correspond to columns, and the variables to be explained (y-axis) correspond to rows. Red highlights significant regressions that explain more than 50% of the variance ( $R^2 > 50\%$ ). Blue highlights regressions that are significant ( $p < 0.01$ ) but that explain less than 50% of the variance. The values used for Normalized Decorrelation, i.e.  $(R_{input} - R_{output}) / R_{input}$ , and for Spiketrain Reliability ( $R_w$ ) were computed with a binning window of 10 ms, unless specified.

**Table 1. Intrinsic electrophysiological cell properties**

		x-axis →			
		Membrane Capacitance (Cm)	Membrane Resistance (Rm)	Membrane Time Constant = Rm.Cm	Resting Membrane Potential (Vrest)
<b>Normalized Decorrelation</b>	<b>GC</b>	$R^2 = 4\%$ $p = 0.08$ slope = -0.2	$R^2 = 5\%$ $p = 0.06$ slope = -0.03	$R^2 = 8\%$ $p = 0.013$ slope = -1.2	$R^2 = 3\%$ $p = 0.17$ slope = -0.2
	<b>FS</b>	$R^2 = 47\%$ $p = 0.0008$ slope = -1.5	$R^2 = 77\%$ $p < 0.0001$ slope = 0.6	$R^2 = 5\%$ $p = 0.4$ slope = 13.6	$R^2 = 46\%$ $p = 0.0009$ slope = 1.4
	<b>GC + FS</b>	$R^2 = 1\%$ $p = 0.3$ slope = -0.1	$R^2 = 4\%$ $p = 0.05$ slope = 0.04	$R^2 = 1\%$ $p = 0.4$ slope = -0.07	$R^2 = 0.1\%$ $p = 0.7$ slope = -0.1
<b>Spiketrain Reliability (<math>R_w</math>)</b>	<b>GC</b>	$R^2 = 2\%$ $p = 0.2$ slope = 0.001	$R^2 = 5\%$ $p = 0.03$ slope = $4e-3$	$R^2 = 7\%$ $p = 0.02$ slope = 0.01	$R^2 = 3\%$ $p = 0.17$ slope = 0.002
	<b>FS</b>	$R^2 = 48\%$ $p = 0.0006$ slope = 0.01	$R^2 = 70\%$ $p < 0.0001$ slope = -0.007	$R^2 = 6\%$ $p = 0.29$ slope = -0.12	$R^2 = 39\%$ $p = 0.003$ slope = -0.014
	<b>GC + FS</b>	$R^2 = 0.7\%$ $p = 0.4$ slope = 0.001	$R^2 = 3\%$ $p = 0.07$ slope = $-4e-5$	$R^2 = 1\%$ $p = 0.37$ slope = $8e-4$	$R^2 = 0.1\%$ $p = 0.7$ slope = $8e-4$

**Table 2. Spike-wise neural noise**

		x-axis →			
		Delay	Jitter	Spiking Reliability (SR)	
Normalized Decorrelation	GC	$R^2 = 39.5\%$ $p < 0.0001$ slope = 1.8	$R^2 = 43\%$ $p < 0.0001$ slope = 1.3	$R^2 = 45\%$ $p < 0.0001$ slope = -47.3	
	GC, 100ms	$R^2 = 2\%$ $p = 0.3$ slope = 0.7	$R^2 = 13\%$ $p = 0.01$ slope = 1.2	$R^2 = 41\%$ $p < 0.0001$ slope = -72	
	FS	$R^2 = 13\%$ $p = 0.1$ slope = 2.2	$R^2 = 22\%$ $p = 0.04$ slope = 9.2	$R^2 = 88\%$ $p < 0.0001$ slope = -42.4	
	Shuffle	$R^2 = 11\%$ $p = 0.02$ slope = 0.9	$R^2 = 24\%$ $p = 0.0003$ slope = 0.8	$R^2 = 65\%$ $p < 0.0001$ slope = -41.1	
	Spiketrain Reliability ( $R_w$ )	GC	$R^2 = 33\%$ $p < 0.0001$ slope = -0.016	$R^2 = 43\%$ $p < 0.0001$ slope = -0.013	$R^2 = 46\%$ $p < 0.0001$ slope = 0.5
		GC, 100ms	$R^2 = 3\%$ $p = 0.2$ slope = -0.008	$R^2 = 16\%$ $p = 0.004$ slope = -0.012	$R^2 = 43\%$ $p < 0.0001$ slope = 0.7
		FS	$R^2 = 15\%$ $p = 0.09$ slope = -0.024	$R^2 = 15\%$ $p = 0.09$ slope = -0.078	$R^2 = 85\%$ $p < 0.0001$ slope = 0.4
		Shuffle	$R^2 = 9\%$ $p = 0.04$ slope = -0.008	$R^2 = 23\%$ $p = 0.0004$ slope = -0.008	$R^2 = 65\%$ $p < 0.0001$ slope = 0.4



**Table 3. Spiketrain-wise properties**

		x-axis →	
		Overall Firing Rate	Spiketrain Reliability ( $R_w$ )
<b>Normalized Decorrelation</b>	<b>GC</b>	$R^2 = 15\%$ $p < 0.0001$ slope = - 1.27	$R^2 = 81\%$ $p < 0.0001$ slope = -87
	<b>FS</b>	$R^2 = 65\%$ $p < 0.0001$ slope = - 0.50	$R^2 = 90\%$ $p < 0.0001$ slope = -85
	<b>GC + FS</b>	$R^2 = 47\%$ $p < 0.0001$ slope = - 0.80	$R^2 = 90\%$ $p < 0.0001$ slope = -90